TÉCNICO LISBOA

Microkinetic modeling applied to catalytic cracking of paraffins

Pedro Miguel Lopes Gomes

Thesis to obtain the Master of Science Degree in

Chemical Engineering

Supervisors:

Prof. Francisco Manuel da Silva Lemos

Prof. Maria Amélia Nortadas Duarte de Almeida Lemos

Examination Committee

Chairperson: Prof. Carlos Manuel Faria de Barros Henriques

Supervisor: Prof. Francisco Manuel da Silva Lemos

Members of the Committee: Prof. José Manuel Félix Madeira Lopes

June 2018

Acknowledgements

I would like to express my gratitude to Professors Francisco Lemos and Amélia Lemos, for all the dedication and support provided throughout the development and elaboration of this work.

To my laboratory colleagues: João Loios, Everton Santos, Hugo Pinto, Tiago Caracol and Daniela Santos, I would like to thank for the good environment in my workplace and also for their support and advices.

From the previous ones mentioned I would like to give a special thanks to João due to our scientific discussions which were very helpful for me.

I also would like to thank to other friends: Mónica Catarino, Diogo Neto, Bruno Melo, Ruben Santos, Sofia Capelo and Ricardo Matias, which somehow helped me in the elaboration of this work by giving me good advices, support and motivation.

Last but not least, I would like to give a special thanks to my parents for all the support they gave me and also for financing me throughout this journey.

THIS PAGE WAS INTENTIONALLY LEFT BLANK

Abstract

In order optimize the efficiency of the FCC process for a certain target, a better understanding of its complex reaction network is required.

The purpose of this work is to develop a microkinetic lumped model with a small parameter set, capable of making accurate and detailed predictions of the product distribution for the catalytic cracking of paraffins, independently of their size which could later be applied to real FCC feedstocks.

To reduce the number of individual rate constants, these are organized by reaction families and calculated through empirical equations based on the nature of species involved and of the reaction involved, while the lumps are organized by number of carbon atoms and by chemical family.

The model is fitted to experimental results using n-heptane with a partial pressure in the feed of 0.42 atm and then tested for different partial pressures of the same reactant and of n-hexane and n-octane. The experimental data corresponds to catalytic cracking over an H-ZSM-5 catalyst.

The model still requires further development, mainly in the prediction of the molar fraction of propane which is one of the main product for these feedstocks. This is clear in the simulations for n-heptane and n-octane. However, in the simulations for n-hexane, the model can make a good prediction of the molar fractions not only of propane, but also the rest of the product distribution. This may indicate that the problem should be related to the symmetry of the protolytic scission reaction.

Keywords: catalytic cracking, microkinetic model, lumped model, paraffins, olefins, aromatics

THIS PAGE WAS INTENTIONALLY LEFT BLANK

Resumo

Para otimizar a eficiência do processo da FCC para um determinado objectivo, é necessário um melhor entendimento de sua complexa rede reacional.

O objetivo deste trabalho é desenvolver um modelo microcinético de lumps com um pequeno conjunto de parâmetros, capaz de fazer previsões precisas e detalhadas da distribuição do produto para o cracking catalítico de parafinas, independentemente do seu tamanho, que poderia ser aplicado posteriormente a matérias-primas reais de FCC.

Para reduzir o número de constantes de velocidade individuais, estas são organizadas por famílias de reação que são calculadas através de equações empíricas baseadas na natureza das espécies envolvidas e da reação envolvida, enquanto os lumps são organizados por número de átomos de carbono e por família química.

O modelo é ajustado a resultados experimentais usando n-heptano com uma pressão parcial na alimentação de 0,42 atm e depois testado para diferentes pressões parciais do mesmo reagente e de n-hexano e n-octano. Os dados experimentais correspondem ao cracking catalítico usando o H-ZSM-5 como catalisador.

O modelo ainda requer desenvolvimento adicional, principalmente na predição da fração molar de propano, que é um dos principais produtos para estas matérias-primas. Isso fica claro nas simulações de n-heptano e n-octano. No entanto, nas simulações para n-hexano, o modelo consegue fazer uma boa previsão das frações molares, não apenas do propano, mas também do restante da distribuição do produto. Isso pode indicar que o problema deve estar relacionado com a simetria da reação de cisão protolítica.

Palavras-chave: cracking catalítico, modelo microcinético, modelo de lumps, parafinas, olefinas, aromaticos

THIS PAGE WAS INTENTIONALLY LEFT BLANK

Table of Contents

List of Figures

List of Tables

List of Abbreviations

FCC – fluid catalytic cracking

LPG – liquefied petroleum gas

PCP – protonated cyclopropane

H_2 – molecular hydrogen

C_x – hydrocarbon with x atoms of carbon

n-Paraffin – linear paraffin

i-Paraffins – branched paraffin

n – number of carbon atoms used in elementary step reactions

m - number of carbon atoms used in elementary step reactions

i – number of carbon atoms used elsewhere

j – type of molecule

P_x – paraffin with x atoms of carbon

O_x – olefin with x atoms of carbon

A_x – aromatic with x atoms of carbon

nP_x – linear paraffin with x atoms of carbon

iP_x – branched paraffin with x atoms of carbon

k_f – rate constant for forward reaction of isomerization

k_r - rate constant for reverse reaction of isomerization

$k_{ps(n,m)}$ – rate constants for protolytic scission

$k_{bs(n,m)}$ – rate constants for β-scission

$k_{cg(n,m)}$ – rate constants for chain growth

$k_{ht(n,m)}$ – rate constants for hydride tranfer

$k_{ar(n,m)}$ – rate constants for aromatic formation

K – isomerization equilibrium constant

$K_{(n)}$ – sum of isomerization equilibrium constants

$N_{(i,j)}$ – number of moles for a compound with i carbon atoms form the j type

$F^e_{(i,j)}$ – inlet molar flow for a compound with i carbon atoms form the j type

$F^o_{(i,j)}$ – outlet molar flow for a compound with i carbon atoms form the j type

$r_{(i,j)}$ – global reaction rate for a compound with i carbon atoms form the j type

$r_{ps(n,m)}$ – elementary step reaction rates for protolytic scission

$r_{bs(n,m)}$ – elementary step reaction rates for β-scission

$r_{cg(n,m)}$ – elementary step reaction rates for chain growth

$r_{ht(n,m)}$ – elementary step reaction rates for hydride tranfer

$r_{ar(n,m)}$ – elementary step reaction rates for aromatic formation

$r_{iso(n)}$ - elementary step reaction rates for isomerization

$P_{(i,j)}$ – partial pressure for a compound with i carbon atoms form the j type

F_t^e – inlet total molar flow

F_t^o – outlet total molar flow

t – time

N_{inert} – number of moles for inerts

P_t – Total pressure

$[nP]_{eq}$ – linear paraffins concentration at equilibrium state

$[iP]_{eq}$ – branched paraffins concentration at equilibrium state

Δt – time increase

ΔG_r – free energy of Gibbs of reaction

ΔG_f – free energy of Gibbs of formation

ΔH_f – enthalpy of formation

ΔS_f – entropy of formation

T – temperature

R – ideal gases constant

1 Context and Objectives

The increasing demand for higher quality fuels to match the market needs led to the implementation of conversion processes in oil refineries in order to convert oil's heavier fractions to increase light products and middle distillates fractions [1]. This increasing demand was accompanied by the need for better quality fuels that was originated by environmental concerns such as the reduction of emissions, public health concerns with the approval of legislations which prohibited certain substances in fuels such as aromatics and lead in gasoline whose was proven to cause cancer or even performance concerns due to needs of the newer engines. Last but not least, economic concerns such as the decreasing oil availability, while compared to its consumption, and the need to maintain adequate fuel prices led to the implementation of these conversion processes [2][3].

Since the 1940's, catalytic cracking has been one of the most important of these processes due to the flexibility of its feedstocks which can come from a large variety of processes inside the refinery. Also, different types of oil lead to different fractions of products which can be adjusted using catalytic cracking [4].

According to the 2018 edition of BP Energy Outlook [5], the liquid fuels demand will increase over the next years, reaching a peak in mid 2030s. This increase in liquid fuels demand is being driven by the sector of transports. Despite predictions of a small decrease on this demand in the late 2030s, the main source of fuel in the transport sector will continue to be oil. This decrease in the demand for liquid fuels occurs due to two big factors: the expected growth of the electric cars market [6] and the decrease of new diesel cars sales [7]. Both factors are related to the new policies adopted by many developed countries to face the current environmental situation [6][7]. Once combining all these factors, it can be deduced that the increasing demand will be met by gasoline and other alternative fuels.

Nowadays, fluid catalytic cracking is the most used process to convert high boiling point products into lighter compounds such as gasoline and lighter products [8][9]. Some of them to be directly blended in gasoline pool of the refineries and others to be fed in deep conversion processes such as: alkylation, isomerization and esterification, in order to produce high octane number compounds for gasoline blending [10]. However, despite all the research conducted on the area about catalytic cracking there is no model yet to accurately predict a detailed product distribution of FCC processes depending only on the feed composition, the catalyst and the operating conditions, which are of great importance in order to optimize the process. To do so, its complex reaction network must be studied and fully understood through the development of kinetic models.

The purpose of this work is to develop a semi-empirical kinetic model to make a detailed prediction of the product distribution for catalytic cracking based on the number of carbon atoms and the type of compound. The model was developed using pure n-heptane as reactant and it was then tested for n-hexane and n-octane.

THIS PAGE WAS INTENTIONALLY LEFT BLANK

2 State of the Art

2.1 Evolution of Catalytic Cracking

Catalytic cracking is a process within an integrated refinery used to convert the high boiling point fractions from oil into lighter products, namely gasoline [10].

Since its introduction in oil refineries, catalytic cracking processes has undergone several modifications in order to improve its efficiency and allow an easier adaptation to the market demands. The first catalytic cracking unit was an old thermal cracker converted into a catalytic cracker in 1936 producing 2,000 barrels per day of oil. This unit used the Houdry's process which used semi-batch reactors with fix bed of catalyst. The total capacity of units in operation using Houdry's process in 1940 was 140,000 bpd of oil [10].

Catalytic cracking required relatively frequent regeneration of the catalyst and, in order to turn the catalytic cracking semi-batch processes into continuous processes the thermofor catalytic cracking (TCC) was developed. This was a moving bed process which used a conveyor to move the catalyst from the regenerator to the reactor. The first TCC unit started to operate in 1943 producing 10,000 bpd and by the end of World War II, the total capacity of this type of units was 300,000 bpd [10].

Meanwhile, an alternative process to Houdry's process was being developed. This process is called fluid catalytic cracking (FCC). On FCC process a low velocity gas passing through the catalyst in powder form, carries it from the regenerator to the reactor, and beck again, and fluidizes it. [10].

The first commercial FCC unit started operation in 1942 producing 12,000 bpd of oil [10] and since then the process has undergone several modifications in terms of: design of the process, mechanical improvements, catalysts used and also the processing objectives, in order to improve its efficiency and to adapt to the market needs and legislations [11].

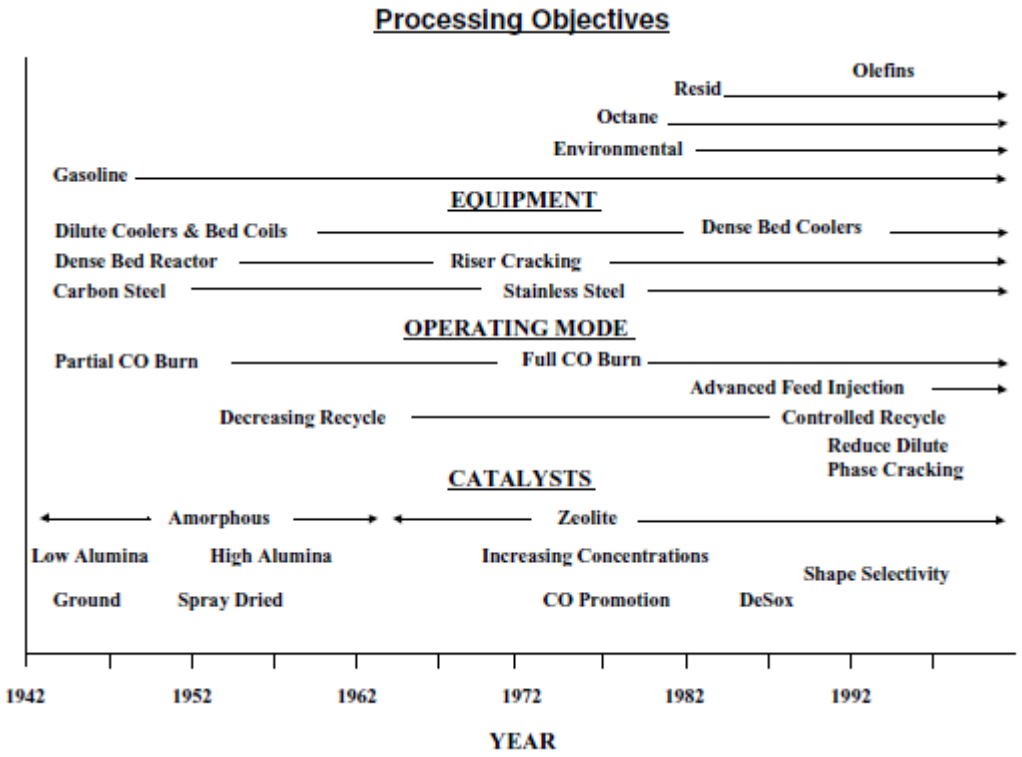

Figure 1 - Evolution of FCC Process [11].

Nowadays FCC is the most used conversion process to transform the heavier fractions into gasoline and light olefins (C_3-C_4). In 2012 there were around 350 FCC units operating worldwide, processing 14.7 million bpd [10].

2.2 FCC Process

The FCC process have suffered several modifications throughout the years by the different technology licensors but a general schematic diagram of the process is presented in Figure 2.

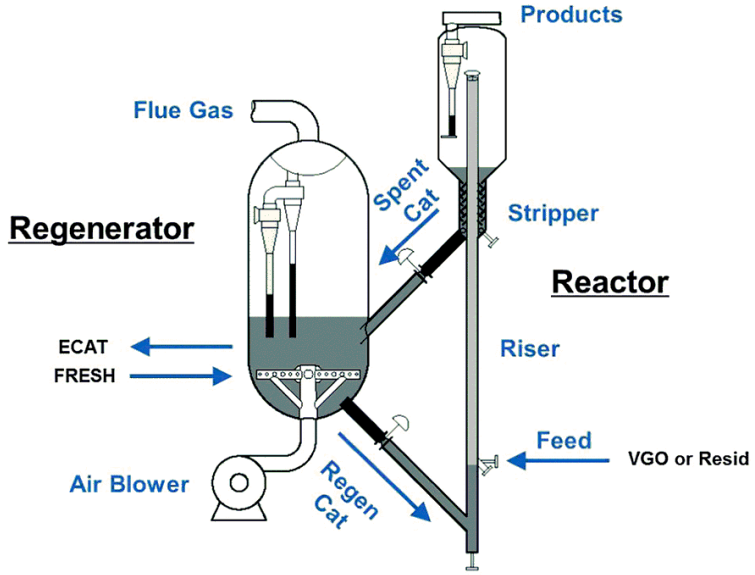

Figure 2 - General schematic diagram of the FCC process (adapted) [12].

2.2.1 Feed Preheat

Prior to the process there is a surge drum for blending of FCC feedstocks. This drum can also suit to separate any eventual water or vapor present in FCC feedstocks [10].

Also prior to the process, the feed is preheated with hot streams, generally with pumparound streams coming from the main fractionator, allowing to do an energetic integration between the feed and products due to their enthalpic needs. Feed's heat demand can came from other sources to maximize the preheat temperature. These sources are generally fired heaters and the flue gas coming from the regenerator which allows to control the temperature inside the regenerator [10].

2.2.2 Feed Nozzles and Riser

After the preheating zone, the feed goes to the reactor, the riser. Prior to entering in the riser, the feed is atomized in the feed nozzles, through dispersion or atomizing steam, to promote a better contact between the feed and the catalyst. When the feed enters the riser contacts with the hot regenerated catalyst and vaporizes. The heat provided by the catalyst is enough to vaporize the feed and increase its temperature to cracking temperatures. The cooling that occurs throughout the riser due to the global endothermicity of reaction network is also balanced with the heat transferred by the regenerated catalyst. The riser's operation can adequately be described by plug flow reactor with minimal mixing, whereby catalyst and vapor ascend driven by the vapor's volume expansion. Coke is also formed during the permanence of the catalyst inside the riser, which, despite the negative effect of deactivating the catalyst, is actually of great importance for the overall energy balance of the entire process [10].

2.2.3 Catalyst Separation

After the catalyst and the vapor leave the riser they enter in a vessel which acts as a separation zone for catalyst and vapor. Many configurations exist for this stage of process. In most of cases there is an initial separation to separate most of the catalyst from the vapor using the inertia due to a change in the flow direction in which the catalyst descend to the stripping section. This can be done with or without a deflector device. The vapor and the remaining particles flow to system of cyclones to separate them, which can be single-stage or two-stage. In some cases the end of the riser is directly connected do the cyclones. The vapor ascends through the top of the cyclones to the main fractionator in order to separate the products while the catalyst descend to a stripping section with the help of diplegs [10].

2.2.4 Stripping Section

The main stripping section has the purpose to remove the vapors with high hydrogen to carbon ratio inside the catalyst's pores. This is performed with an up flow of high temperature steam which carry these hydrocarbon vapors. There are also hydrocarbons adsorbed in the catalyst's surface and pores. These are not removed with stripping stream but due to the high temperatures and the catalyst high residence times inside stripping section cracking reaction still happen and convert these adsorbed hydrocarbons into light products. The level of catalyst inside the stripping section is controlled by a side or plug valve in order to prevent a flow of flue gas from the regenerator into the reactor [10].

2.2.5 Catalyst Regenerator

After passing through the stripping zone the catalyst goes to the regenerator. In the regenerator the coke adsorbed or trapped in the catalyst is burned to restore the catalytic activity and to increase the catalyst temperature so he can act as a heat supplier inside the riser. The oxygen required for the combustion is supplied by air blowers in bottom of regeneration vessel which has also the role to maintain the catalyst bed in a fluidized state [10].

The regenerator's efficiency is limited by temperature. Feedstocks with high content of residue decrease the process yield because the amount of coke adsorbed to the catalyst is much higher. Due to safety measures, the combustion of coke must be incomplete which will cause a significant decrease in the number of active sites on regenerated catalyst. Also, it is important to minimize the amount of hydrocarbons inside the regenerator because the combustion of compounds containing high content of hydrogen, apart from constituting a waste in production, produces considerably more heat than the combustion of coke. So, in order to control the temperature of the regenerator the feed rate may have to be decreased likewise the production of the process [10].

2.2.6 Regenerator Outlet Streams

The flue gas leaves the top of the regenerator through a system of cyclones which separate the flue gases from catalyst particles carried by the gas. As it was previously said, the flue gas can be used as hot stream to perform an energy integration scheme [10].

The regenerated catalyst leaves the bottom of the regenerator to return to the riser through a standpipe which may or may not have external aeration to maintain the catalyst fluidized, depending on standpipe's length. In order to ensure that the energetic requirements inside the riser, the incoming regenerated catalyst flow rate is controlled with slide or plug valve which is controlled by the riser's temperature. Despite the efficiency of both systems of cyclones being close to 100%, there is some catalyst loss whereby it is required to do make-ups of catalyst [10].

2.3 FCC Feedstock Composition

FCC most usual feedstock is the vacuum distillate, vacuum gas oil (VGO) which may be blended with residues and other gas oils produced in the refinery [13]. FCC feedstocks can be presented to a variable levels of hydrotreatment [10].

FCC feedstocks are mainly composed by paraffins, olefins, naphthenes and aromatics. Paraffins are saturated hydrocarbons and are the main component of FCC feedstocks. Olefins are unsaturated hydrocarbons and much more reactive when compared to paraffins. Olefins appear in FCC feedstocks coming from other processes inside the refinery since they do not appear in crude oil. Naphthenes are cyclic paraffins. Aromatics are cyclic unsaturated hydrocarbons stabilized by resonance with at least one ring [10].

FCC feedstocks can also contain impurities and their concentration depends on three main factors: the origin of the crude oil, how much residue has been blended to the feedstock and how much the feedstock has been previously hydrotreated. These impurities usually are heavy organic compounds, coming mostly form the blended residues and that may contain sulfur, nitrogen and metals like: copper, calcium, iron, potassium, vanadium and nickel. These impurities, apart from sulfur, cause deactivation in the catalyst by poisoning which leads to a loss in the conversion of the feed. Sulfur's main problem is related to an increase of hydrotreatment costs to meet product specifications and environmental regulations [10].

2.4 FCC Products

The FCC process has many different products, being organized in groups organized by range of boiling point [10]:

- Dry gas (H_2 and C_1 to C_2);
- LPG (C_3 to C_4);
- Gasoline;
- Light cycle oil (LCO) to be blended with diesel;
- Heavy cycle oil (HCO);
- Slurry.

The relative amounts of each product varies with several factors, such as: the quality of the feedstock, the operating conditions and catalysts, which also are adjusted according to the market conditions [10][14].

FCC main products were, conventionally, mostly gasoline and also LPG [8][10]. However, more recently refiners are decreasing gasoline yield to favor light olefins yield, mainly propylene, due to the increasing demand of this product in the petrochemical industry[14][15]. Despite the amount of gasoline produced being lower, its quality is higher due to an increase in octane number

[14]. The octane number is the property of gasoline that is used to evaluate the resistance to knocking and is calculated as the volume percentage of i-octane in a binary blend with n-heptane which produces the same knock intensity as that gasoline under standard conditions [16].

Although coke is also a product, it does not leave the process as such, being adsorbed to the catalyst after the reaction. Coke is formed in the riser and it is burned in the regenerator to reactivate the catalyst [10].

2.5 FCC Catalyst

Nowadays FCC catalysts are constituted by a support matrix incorporating zeolites, mainly Y and its variations: rare-earth Y (REY) and ultra-stable Y (USY); and ZSM5 [10].

Zeolites are crystalline structures composed by a network of tetrahedra with oxygen atom at the corners and an atom of aluminum or silicon in the center. The ratio Si/Al in zeolite varies from zeolite to zeolite [10].

The active sites in zeolite are associated with the aluminum atoms because of the negative net charge they introduce in the framework imparting to its tetrahedron an acid nature. The strength of an acid sites increases with the distance to other acid sites [17] [18] which affects not only their activity, but also their selectivity. Assuming a uniform distribution of acid sites, higher Si/Al ratios tends to have lesser acid sites but stronger ones [19]. Stronger acid sites favor the production of the light olefins and increase the gasoline octane number [10][20].

FCC zeolites, due to their structure, have a framework of micropores which allows them to effect shape selectivity allowing the smaller hydrocarbons to enter in the pores and react while bigger ones cannot enter [21].

Besides serving as support for the zeolite, the matrix also acts as a source of primary cracking for the heavier hydrocarbons that cannot enter the zeolite pores. The matrix is usually composed by silica and alumina, the last one being the source of active sites, but, unlike the zeolite, it has an amorphous structure [10].

Deactivation of a FCC catalyst can occur due three factors: thermal degradation, poisoning and coke deposition.

Deactivation by coke deposition, as explained before, is a necessary evil to maintain the overall energy balance of the process. Coke is composed by condensed hydrocarbon compounds with low content of hydrogen, mainly aromatics [9]. The deposited coke blocks the micropores preventing the diffusion of hydrocarbons inside them [22], adsorbs at the acid sites [21] or both [9]. However, this deactivation is temporary since the coke is removed in the regenerator and catalytic activity is restored.

Thermal deactivation occurs due to the conditions to which the catalyst is presented inside the regenerator and is represented by a loss of alumina from the zeolite structure. These effects can be enhanced by the presence of Sodium in the zeolite structure or reduced through the addition of rare earth elements to stabilize aluminum atoms [10].

Deactivation by poisoning occurs due to the presence of certain impurities on the feedstock: nitrogen compounds and some metals such as vanadium, nickel and sodium. In the case of nitrogen, these compounds have a basic nature and will react with the acid sites [20] or even act as coke precursors [9] causing a temporary loss activity. However, most of these can be removed in the regenerator [10]. In the case of metals like vanadium, nickel and sodium; these metals deposit on the matrix and external surface of the zeolite, in case of nickel [23], and inside the structure of the zeolite, in the case of vanadium and sodium [18][24][25]. Parasite reactions, such as dehydrogenation and polymerization, are promoted by nickel [23][25] while destabilization of the zeolite crystalline structure is promoted by vanadium and sodium [24][25]. Sodium also neutralizes acid sites [18][19]. These effects results in a permanent loss of catalytic activity and in the second case it can cause the disintegration of the zeolite structure inside the regenerator [18][23][24][25].

2.6 FCC Reactions

There is a wide range of reactions in the FCC process. In Figure 3 is presented a resume of some of the important reactions in the FCC process and some examples.

1.	Cracking:	
	Paraffins cracked to olefins and smaller paraffins	$C_{10}H_{22} \rightarrow C_4H_{10} + C_6H_{12}$
	Olefins cracked to smaller olefins	$C_9H_{18} \rightarrow C_4H_8 + C_5H_{10}$
	Aromatic side-chain scission	$ArC_{10}H_{21} \rightarrow ArC_5H_9 + C_5H_{12}$
	Naphthenes (cycloparaffins) cracked to olefins and smaller ring compounds	Cyclo-$C_{10}H_{20} \rightarrow C_6H_{12} + C_4H_8$
2.	Isomerization:	
	Olefin bond shift	1-$C_4H_8 \rightarrow$ trans-2-C_4H_8
	Normal olefin to iso-olefin	n-$C_5H_{10} \rightarrow$ iso-C_5H_{10}
	Normal paraffin to isoparaffin	n-$C_4H_{10} \rightarrow$ iso-C_4H_{10}
	Cyclohexane to cyclopentane	$C_6H_{12} + C_5H_9CH_3$
3.	Hydrogen transfer:	Naphthene + olefin → aromatic + paraffin
	Cycloaromatization	$C_6H_{12} + 3C_5H_{10} \rightarrow C_6H_6 + 3C_5H_{12}$
4.	Transalkylation/alkyl-group transfer	$C_6H_4(CH_3)_2 + C_6H_6 \rightarrow 2C_6H_5CH_3$
5.	Cyclization of olefins to naphthenes	$C_7H_{14} \rightarrow CH_3$-cyclo-$C_6H_{11}$
6.	Dehydrogenation	n-$C_8H_{18} \rightarrow C_8H_{16} + H_2$
7.	Dealkylation	Iso-C_3H_7-$C_6H_5 \rightarrow C_6H_6 + C_3H_6$
8.	Condensation	Ar-CH=CH_2 + R_1CH=$CHR_2 \rightarrow$ Ar–Ar + 2H

Figure 3 - Important Reactions Occurring in the FCC Unit and examples [10].

Besides these reactions, there are also others that can occur, like thermal cracking, inside the riser, and coke combustion inside the regenerator.

From the above reactions only the ones presented in the kinetic model proposed in this work will be studied:

- Catalytic cracking of paraffins
- Oligomerization of olefins
- Hydride transfer between olefins and paraffins
- Isomerization of paraffins
- Cycloaromatization

2.6.1 Catalytic Cracking of Paraffins

Catalytic cracking mechanism of paraffins is a matter that has not been yet fully understood although there are some main theories that are generally accepted to explain it.

It is believed that catalytic cracking of paraffins occurs as a chain reaction according to the Whitmore carbenium ion theory [26]. Despite all the discussion about how catalytic cracking is initiated, consensus have been reached about the type of acid sites responsible for the initiation of catalytic cracking: Brønsted acid sites. Brønsted acid sites can ensure some stability to the adsorbed carbenium ion [22] [27]. However, Lewis acid sites also have an important role during the propagation step [28].

Some authors suggested that the formation of the carbenium ions occurs due to the protonation of an olefin present in the feed by a Brønsted acid site [29] followed by a hydride abstraction from a gas phase paraffin to form a new carbenium ion [30]. Later, other authors suggested the formation of a penta-coordinated carbonium ion by direct protonation of paraffin [31].

The classic mechanism for the catalytic cracking is a bimolecular mechanism proposed by Greensfelder [30] and consists on gas phase paraffin carrying out a hydride transfer with a carbenium ion that is already adsorbed which results in a new carbenium ion adsorbed and the desorption of the previous one. The new carbenium ion will then crack, by β-scission producing an olefin and a smaller carbenium ion and this carbenium ion will take part on hydride transfer reactions with some other gas phase paraffin to restart the cycle. A scheme to illustrate this reactional cycle is presented in Figure 4.

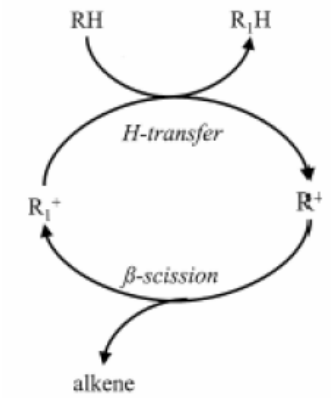

Figure 4 – Reactional cycle of the traditional bimolecular mechanism for catalytic cracking of paraffins [32].

Although this mechanism has been generally accepted, it has some limitations to its applicability: it requires pre-existing carbenium ions and cannot explain the appearance of dry gas in the product distribution.

An alternative mechanism for the initiation step of the catalytic cracking of paraffins as proposed by Haag and Dessau [31] is called protolytic scission. This is a monomolecular mechanism in which strong Brønsted acid site protonates a paraffins, with higher tendency to

happen on the most substituted carbon atom, forming a pentacoordinated carbonium ion. This is a very instable intermediate state and it soon drops a molecule of H_2 or a smaller paraffin to form carbenium ion also smaller than the original paraffin. This alternative mechanism, when compared with the traditional one, has the advantages of not needing the pre-existence of carbenium ions and it can also explain the formation of molecular hydrogen, methane and ethane. A scheme to illustrate the protolytic scission is presented in Figure 5.

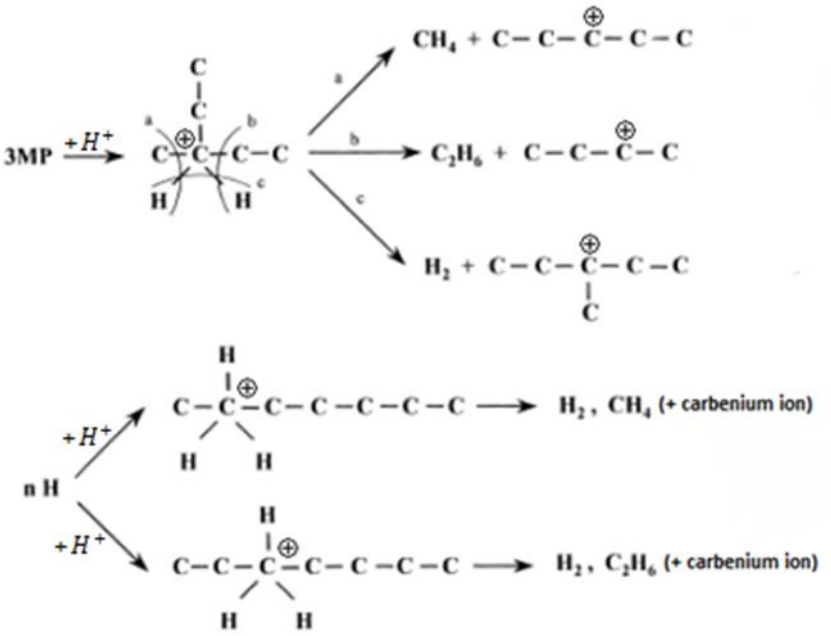

Figure 5 - Protolytic scission mechanism for linear and branched paraffins (adapted) [33].

Although later works by Sommer [34][35][36] concluded that the results were consistent with the protolytic scission for liquid super acids, this initiation mechanism cannot occur easily over a solid acid catalyst. This do not necessarily invalidates the protolytic scission mechanism because the range of temperature for catalytic cracking is far above the one used in those works (25-200ºC) but it shows that the initiation step for the catalytic cracking of paraffins has not yet been fully understood. The most likely real situation is probably a combination of the two main mechanisms – protolytic and carbenium-ion.

More recently, Kissing [37][38] proposed a mechanism in which he differentiates the catalytic cracking of paraffins and olefins. For the catalytic cracking of olefins, he obtained product distributions in accordance with the β-scission mechanism. For the catalytic cracking of isoparaffins he proposed the formation hydrosiloxonium ion as intermediate state in a tertiary carbon. The cracking reaction occurs by the breaking of a C-C bond in the β –position to O^+. This mechanism also predicts the production a large amount of olefins likewise molecular H_2. Like Sommer, Kissing work was performed under very low temperature (150ºC) while comparing with the range of temperature for catalytic cracking. A scheme to illustrate the mechanism proposed by Kissing is presented in Figure 6.

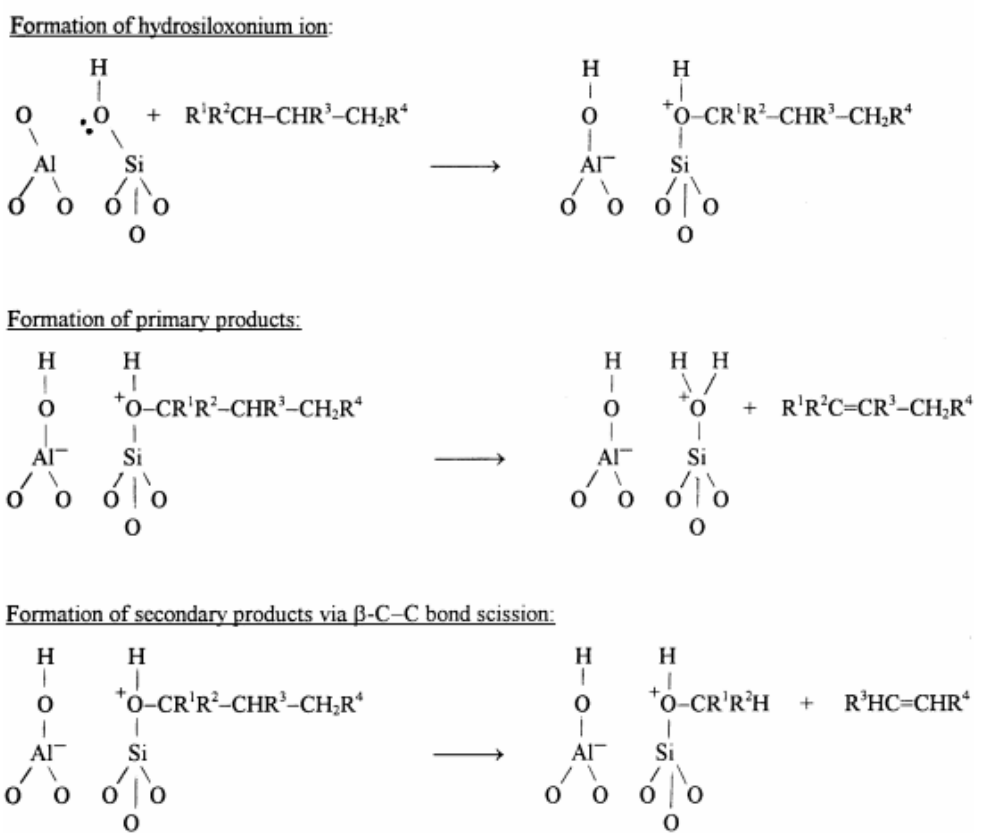

Figure 6 - Mechanism proposed by Kissin for the catalytic cracking of paraffins [38].

The propagation step for the catalytic cracking of paraffins can take several routes, independently of the origin of the initiation step to form the carbenium ion. One possible route is the carbenium ion undergoing β-scission and form a smaller olefin and a smaller carbenium ion than the original one. The carbenium ion can also undergo the traditional bimolecular mechanism by abstracting hydride ion from a paraffin. It can also undergo oligomerization with other olefin forming a bigger carbenium ion. It can also isomerize and then take any of the previous routes [33].

In order to avoid idea of the formation of primary carbenium ions by β-scission because of its high instability, Sie [39][40] proposed a mechanism with a protonated cyclopropane as intermediate (PCP). This mechanism via PCP can explain the presence of a high amount of isoparaffins obtained during the cracking of n-paraffins likewise it avoids the formation of primary carbenium ions. The mechanism via PCP is not applicable for paraffins with less than 7 carbon atoms. For paraffins with less than 7 carbon Sie defends the protolytic scission mechanism proposed by Haag and Dessau [31]. A scheme to illustrate the PCP mechanism is presented in.

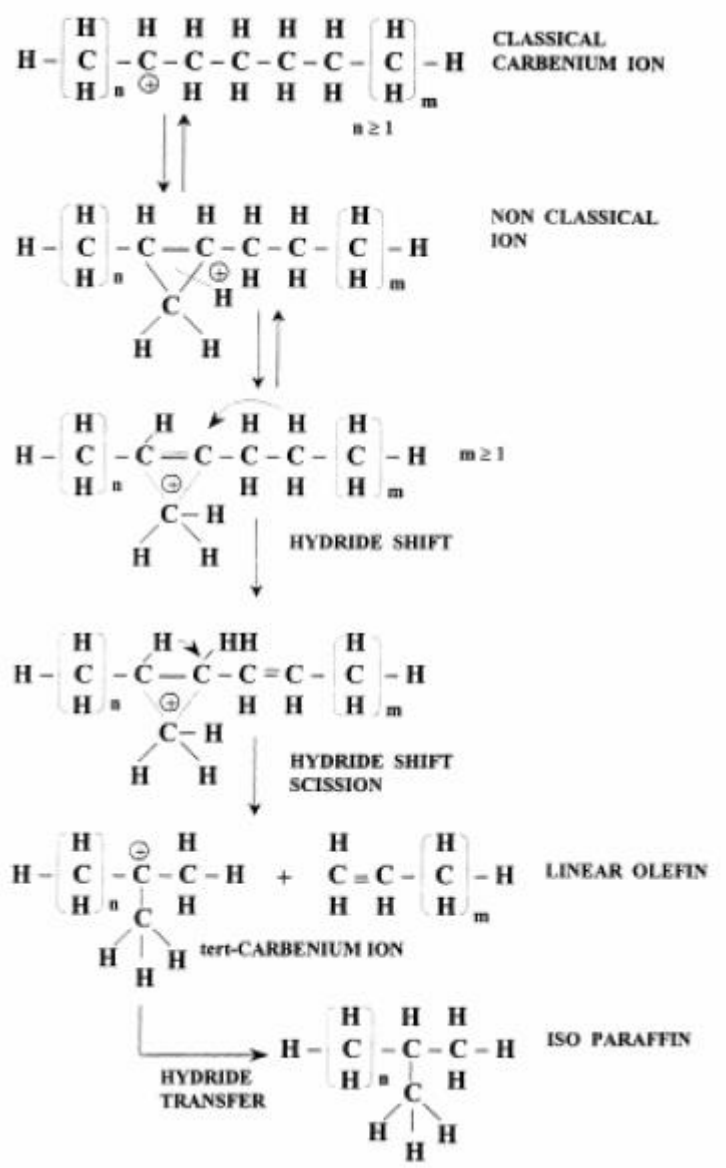

Figure 7 – PCP mechanism for the cracking of normal paraffins [39].

The relative contribution of each of cracking mechanism depends on the nature of the feed, catalyst and operating conditions. Protolytic scission is favored by high temperatures, low partial pressure, low acid site densities and low conversions of reactant [31] while β-scission is favored by lower temperatures [41][42]. Smaller pores have increased shape selectivity and tend to favor protolytic scission because its transition state is smaller than the one from the bimolecular hydride transfer reaction prior to β-scission [33]. This can be observed when comparing ZSM5 with Y, the first one, which has smaller pores, favors the protolytic scission [31]. Also, high Si/Al ratios tend to favor because the protolytic scission because this reactions requires stronger Brønsted acid sites and its strength increase with Si/Al ratio, as explained before, while β-scission is favored by high acid sites concentrations and high adsorption capacity, which decrease with Si/Al ratio [43].

The product distribution will account all these factors since the protolytic scission tends to produce more linear paraffins, methane, ethane, ethylene and molecular hydrogen, while the β-scission tends to produce more branched hydrocarbons according to the PCP mechanism [33].

The carbenium ion can also desorb from the acid site and form an olefin while regenerating the Brønsted acid site. This is considered a termination step for the chain reaction for the catalytic cracking of olefins.

2.7 Available Microkinetic Models

Several microkinetic models have been developed related to catalytic cracking of hydrocarbons. There are 3 types of microkinetic models: mechanistic models, pathways-level models and lumped models [8].

2.7.1 Mechanistic Models

This is the most complex type of microkinetic models. These models accounts a huge amount of molecules likewise the intermediary states which allows them to provide fundamental kinetic information and detailed molecular representation [8]. However, these models require a huge amount of information from experimental data for the estimation of kinetic parameters, which largely increases with the number of reaction steps and the number of species involved [16]. Also, the complexity of these models does not allow them to present a solution in a reasonable time.

Such complexity is unrealistic to apply to gas oil feedstocks converted in a FCC unit due to their high diversity of chemical species present in the feedstock likewise the even higher number of products and intermediates they led to [44].

Although the application of these this type of models catalytic cracking of gas oils feedstocks, they can still be applied to catalytic cracking of pure components. Watson and Klein developed a mechanistic model for catalytic cracking of n-heptane [44]. On this model the reactions are then grouped by families and molecules are grouped by classes which are limited to certain reaction families which leads to establish of a smaller set of parameters to calculate constant rates based on LFER, semiempirical correlations which relates kinetic data to the reacting compounds properties.

2.7.2 Lumped Models

This is simplest type of microkinetic models because it requires less information and consists in grouping compounds with physical and/or chemical properties in common, called lumps, and the kinetic behavior is studied between these groups. This fact makes this type of models the most used in catalytic cracking microkinetic modeling because they very useful when a large number of compounds is being considered. On lumped models related to catalytic cracking,

compounds are usually grouped by ranges of boiling point and sometimes by chemical family [45] while the number of lumps depends on its level of detail that is desired. However, the application of this type of model to the FCC most of times ignores the complexity of its reaction network which limits its application to a specific feedstock [8].

More simple lumped models were developed with three [46][47], four [48][49][50], five [51][52][53], and seven lumps [54] based only in the range of boiling point. However, in all of these models the chemical reactions defined between lumps do not take into account detailed kinetic information which impossibilities a detailed product distribution.

Lumped models based not only in the range of boiling point, but also the chemical family were also developed. An example of this is a model with eight lumps [55]: LCO, gasoline, LPG, dry gas and coke where gasoline was divided into paraffinic, olefin, naphthenic and aromatic. Another example is a model with eleven lumps [56]: coke, heavy oil (HO), diesel oil (DO), gasoline divided into saturates, olefins and aromatics; LPG divided into butylene, propylene and butane with propane; dry gas divided into ethylene and H_2 with paraffinic C_1-C_2. The division of lumps based on range of boiling point by chemical family allows to partially solve the problem mentioned before.

An interesting 22-lump model was developed for hydroisomerization and hydroaromatization of olefins was developed by Chen et al. [16] lumps were organized by chemical structure, and by number of carbon instead of the most used, range of boiling point. The constants rates were estimated using Levenberg–Marquardt algorithm to fit to experimental data.

Pinto [57] developed two lumped models organized by number of carbon atoms and by chemical family: a 61-lump model considering 21 paraffins, 20 olefins and 20 carbenium ions; and 64-lump model considering also 3 aromatic (C_6-C_8). The constant rates were estimated by empirical mathematical expressions whose parameters are related to nature of the reactant species and the nature of reaction itself.

2.7.3 Pathways Models

Pathways models are a kind of compromise between the previous types of microkinetic models. They can make a detailed prediction of the product distribution, which most lumped models cannot, because every observable molecule is accounted in the model. At the same time, this type of microkinetic models can provide a solution in a reasonable time, which mechanistic models cannot, because they do not have in account all the intermediary species reducing drastically the number of chemical species accounted in the model [8].

Kumar developed pathways model for catalytic cracking of gas oils [8]. His model follow the same methodology used by Watson and Klein [44], without accounting intermediary species, but the set of parameters to calculate constant rates were estimated through fitting to experimental data.

THIS PAGE WAS INTENTIONALLY LEFT BLANK

3 Methodology

The methodology used in this work is divided into 2 separate sections: the first related with the development of the microkinetic model and a second one related with isomerization of paraffins.

3.1 Model Development

The pathways approach of the microkinetic model presented in this work is an alternative to mechanistic approach of the model developed by Pinto [57]. This work's model do not have in account the surface species, the carbenium ions. These species are accounted as olefins since the desorption of carbenium ion results in a gas phase olefin and a regenerated Brønsted acid site. Considering this, all the reactions are considered to happen in a pseudo gaseous phase.

Also, the isomerization reaction for paraffins was introduced and therefore the differentiation between linear paraffins and branched paraffins. A more detailed description of the model will be presented further.

3.1.1 Model Description

In this work it is purposed a 60-lump model to study the complex reaction network of catalytic cracking of paraffins. The aim of this model is to make accurate and detailed predictions of the product distribution while using a limited number of parameters. Also, the model predictions should be independent of feedstock composition and the amount of reactant. However, this model is limited to a specific temperature (450 ° C) and catalyst (H-ZSM5).

In order to develop this model, several factors were taken into account:

- The molecules have been lumped by the number of carbon atoms of each compound and by chemical family accounting linear paraffins, branched paraffins and olefins, up to 20 carbon atoms
- The only aromatics accounted for in the model have 6, 7 and 8 carbon atoms.
- The coke formed is accounted as an olefin with 21 carbon atoms which is not accounted for on the flow calculations since it remains adsorbed on the catalyst.
- Intermediary species, such as carbenium and carbonium ions, are not explicitly accounted for in this model and the reactions are considered to happen in a pseudo gaseous phase.
- The model accounts a total of 60 different species (20 n-paraffins, 20 i-paraffins, 20 olefins and 3 aromatics) and 1582 reactions between them.
- Reactions are lumped by families and their constant rates are estimated by empirical equations, one for each family of reactions and with a small set of parameters.

- The rate constants depend only on the size and the nature of the reactant molecules.
- The reaction families considered in the model are:
    - Protolytic scission: a paraffin “cracks” into a smaller paraffin and a olefin with the remaining carbon atoms

$$P_n \xrightarrow{k_{ps}} P_m + O_{n-m} \qquad (1)$$

    - Chain growth: an olefin reacting with other olefin thus forming a bigger one.

$$O_n + O_m \xrightarrow{k_{cg}} O_{n+m} \qquad (2)$$

    - Hydride transfer: abstraction of a hydride ion from a paraffin by an olefin forming an olefin with same number of carbon atoms of reacting paraffin and a paraffin with same number of carbon atoms of reacting olefin (the other hydrogen ion belongs to the catalyst acid site).

$$P_m + O_n \xrightarrow{k_{ht}} O_m + P_n \qquad (3)$$

    - β-scission: the opposite of the chain growth reaction, a bigger “olefin cracks” into 2 smaller olefins.

$$O_n \xrightarrow{k_{bs}} O_m + O_{n-m} \qquad (4)$$

    - Aromatic formation: an olefin cyclizes and transfers 6 hydrogen atoms to 3 olefins forming an aromatic and 3 paraffins. The olefins that cyclizes has 6, 7 or 8 carbon atoms while the 3 olefins that form paraffins have the same carbon atoms.

$$O_m + 3O_n \xrightarrow{k_{ar}} A_m + 3P_n \quad (5)$$

    - Isomerization: a linear paraffin rearranges into a branched paraffin.

$$nP_m \underset{k_r}{\overset{k_f}{\rightleftarrows}} iP_m \quad (6)$$

    - The branched paraffins will also react through protolytic scission and hydride transfer. The products will be linear paraffins and olefins.

$$iP_n \xrightarrow{k_{ps}} \mathrm{n}P_m + O_{n-m} \qquad (7)$$

$$iP_m + O_n \xrightarrow{k_{ht}} O_m + nP_n \qquad (8)$$

3.1.2 Mass Balance

The mass balance to the reactor is described by equation 9, where: the variation of the number of moles throughout the time for a certain compound, with i carbon atoms of the j type, depends on the difference between its entry and outlet flows, and its global reaction rate.

$$\frac{dN_{(i,j)}}{dt} = F^{e}_{(i,j)} - F^{o}_{(i,j)} + r_{(i,j)} \qquad (9)$$

3.1.3 Global Reaction Rates

The global reaction rates for each species is obtained by the sum of all the reaction rates where a certain compound is involved. Equations 10-14 describe the global reaction rates for each type of molecule, where j=1 represents linear paraffins, j=2 represents branched paraffins, j=3 represents olefins and j=4 represents aromatics. The indexes n and m are related to the indexes from equations 1-8.

Linear paraffins:

$$r_{(i,1)} = \sum r_{ps(i=m)} - \sum r_{ps(i=n,1)} + \sum r_{ht(i=n)} - \sum r_{ht(i=m,1)} + 3\sum r_{ar(i=n)} - \sum r_{iso(i=n)} \qquad (10)$$

Branched paraffins:

$$r_{(i,2)} = \sum r_{iso(i=n)} - \sum r_{ps(i=n,2)} - \sum r_{ht(i=m,2)} \qquad (11)$$

Olefins:

$$r_{(i,3)} = \sum r_{ps(i=n-m)} + \sum r_{ht(i=m)} - \sum r_{ht(i=n)} + \sum r_{cg(i=n+m)} - \sum r_{cg(i=n)} - \sum r_{cg(i=m)} + \sum r_{bs(i=m)} + \sum r_{bst(i=n-m)} - \sum r_{bs(i=n)} - \sum r_{ar(i=m)} - 3\sum r_{ar(i=n)} \qquad (12)$$

Aromatics:

$$r_{(i,4)} = \sum r_{ar(i=n)} \qquad (13)$$

Coke:

$$r_{(21,3)} = \sum r_{cg(n+m\geq 21)} \qquad (14)$$

3.1.4 Elementary Step Reaction Rates

The elementary step reaction rates were calculated through equations 15-20, where a generic $k_{(n,m)}$ represents rate constant, w represents the mass of catalyst, and a generic $P_{(i,j)}$

represents the partial pressure of certain specie. The indexes n and m are related to the indexes from equations 1-8.

Protolytic scission:

$$r_{ps(n,m)} = k_{ps(n,m)} \times P_{(n,1\ or\ 2)} \times w \quad (15)$$

Chain growth:

$$r_{cg(n,m)} = k_{cg(n,m)} \times P_{(n,3)} \times P_{(m,3)} \times w \quad (16)$$

Hydride transfer:

$$r_{ht(n,m)} = k_{ht(n,m)} \times P_{(n,3)} \times P_{(m,1\ or\ 2)} \times w \quad (17)$$

β-scission:

$$r_{bs(n,m)} = k_{bs(n,m)} \times P_{(n,3)} \times w \quad (18)$$

Aromatic formation:

$$r_{ar(n,m)} = k_{ar(n,m)} \times P_{(m,3)} \times {P_{(n,3)}}^3 \times w \quad (19)$$

Isomerization:

$$r_{iso} = k_{iso(n)} \left(P_{P_{(n,1)}} - \frac{{}^{P}P_{(n,2)}}{K(n)} \right) \times w \quad (20)$$

The proceeding to calculate the constant rates likewise to calculate the isomerization elementary step reaction rates will be further explain in the results section.

3.1.5 Implementation of the model

In order to implement this model, it was used Euler method through a sub-routine in VBA made from scratch by myself which follows the following set of steps:

Calculate $r_{(i,j)}$ using one the equations 10-14.

Calculate F_t^o using:

$$F_t^o = F_t^e + \sum_{i=1}^{21} \sum_{j=1}^{4} r_{(i,j)} \times V \quad (21)$$

Calculate $F_{(i,j)}^o$ using:

$$F_{(i,j)}^o = F_t^o \times \frac{P_{(i,j)}}{P_t} \quad (22)$$

Calculate $\frac{\Delta N_{(i,j)}}{\Delta t}$ using:

$$\frac{\Delta N_{(i,j)}}{\Delta t} = F_{(i,j)}^o - F_{(i,j)}^e + r_{(i,j)} \quad (23)$$

Calculate the new $N_{(i,j)}$ using:

$$N_{(i,j)}(t + \Delta t) = N_{(i,j)}(t) + \frac{\Delta N_{(i,j)}}{\Delta t}(t) \times \Delta t \quad (24)$$

Calculate the new $P_{(i,j)}$ using:

$$P_{(i,j)} = \frac{N_{(i,j)}}{\sum_{i=1}^{21}\sum_{j=1}^{4} N_{(i,j)} + N_{inert}} \times Pt \qquad (25)$$

A Flowchart of the sub-routine is presented in Figure 8.

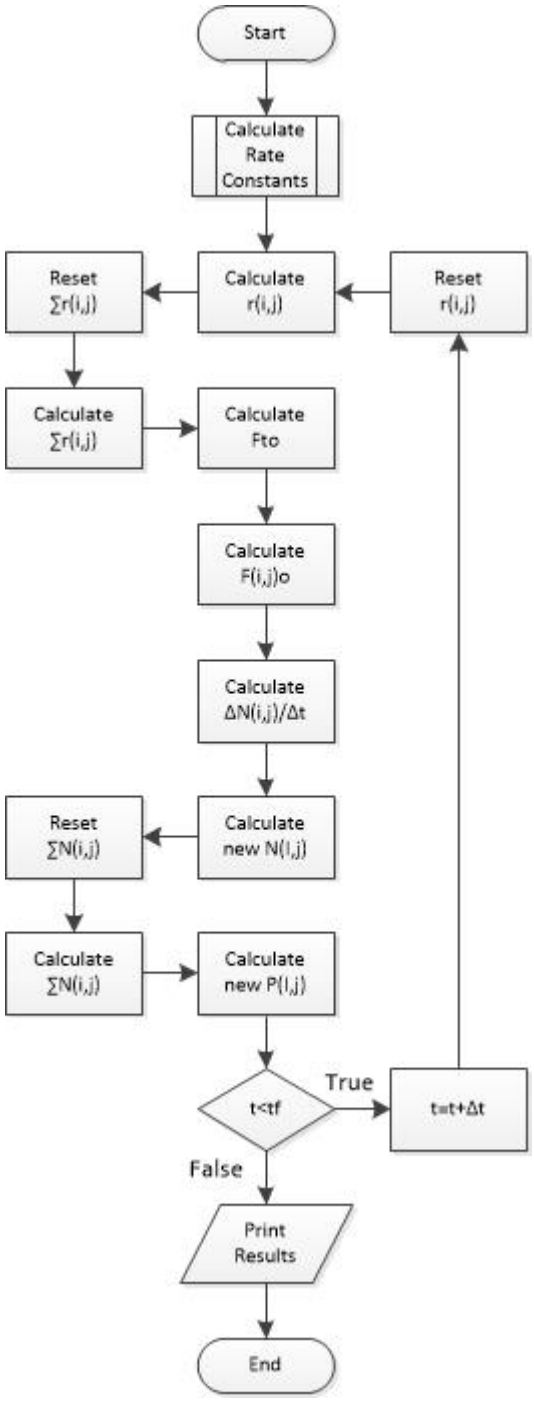

Figure 8 - Model's implementation sub-routine flowchart.

3.2 Isomerization

3.2.1 Isomerization Equilibrium Constant

Isomerization is a first order reversible reaction (equation 6) and its equilibrium constant is expressed through the division of the product concentration by the reactant concentration, when both are at equilibrium:

$$K = \frac{[iP]_{eq}}{[nP]_{eq}} \quad (26)$$

The equilibrium constant can also be expressed by the following thermodynamic equation:

$$K = exp\left(-\frac{\Delta G_r}{RT}\right) \quad (27)$$

where R is the ideal gas constant, T is the temperature (K) and ΔG_r represents the Gibbs free energy variation of the reaction for a given temperature which in turn can be expressed as the difference between the Gibbs free energy of the formation of products and reactants at that temperature:

$$G_r = \Delta G_f(Products) - \Delta G_f(Reactants) \quad (28)$$

In turn, the Gibbs free energy of formation is defined by:

$$\Delta G_f = \Delta H_f - T \times \Delta S_f \quad (29)$$

where H is enthalpy of formation of a given compound, S is his entropy of formation and T is the temperature (K).

In order to determine the enthalpies and entropies all the isomers of paraffins between C_4-C_8 (except 2,2,3,3-tetra-methyl-butane) were simulated at standard conditions for temperature and pressure using *Spartan'06* developed by Wavefunction®. The program used the RB3LYP method and the 6-31G(D) set with 68 shells and 156 basis functions. The results of these simulations are presented in Appendix I.

The equilibrium constants were calculated for every reaction with a linear paraffin as reactant and a different isomer as product using equations 27-29.

Then was plotted the variation of the sum of isomerization equilibrium constants for each number of carbon atoms with the number of carbon atoms (Figure 9).

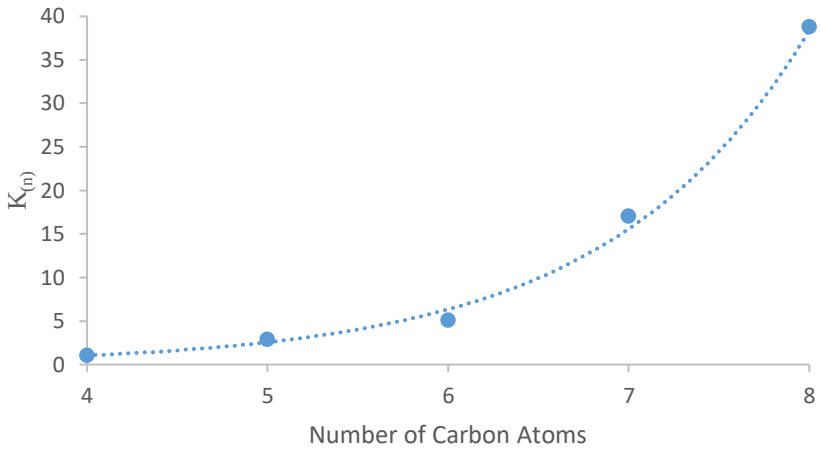

Figure 9 - Variation of the sum of the equilibrium constants with the number of carbon atoms.

The mathematical expression that correlates these 2 variables, $K_{(n)}$, was obtained through fitting the data to an exponential trendline and is presented equation 30. The coefficient of determination that measures how well correlation fits the data is presented in equation 31.

$$K_{(n)} = 0.0284e^{0.901n} \qquad (30)$$

$$R^2 = 0.9916 \qquad (31)$$

3.2.2 Isomerization Elementary Step Reaction Rate

The equilibrium constant can also be defined by ratio between the rate constants of forward and reverse reactions, through equation 32.

$$K = \frac{k_f}{k_r} \qquad (32)$$

The isomerization elementary step reaction rate, r_{iso}, was defined through equation 33.

$$r_{iso} = (k_f P_{nP_m} - k_r P_{iP_m}) \times w \qquad (33)$$

In equation 33 k_r is replaced by equation 32, with k_f being put in evidence, giving place to equation 34:

$$r_{iso} = k_f \left(P_{nP_m} - \frac{P_{iP_m}}{K}\right) \times w \qquad (34)$$

The forward rate constant, k_f, was renamed to k_{iso} which will further explain in the results section. The equilibrium, K, was replaced by correlation obtain previously, $K_{(n)}$, reaching equation 20.

THIS PAGE WAS INTENTIONALLY LEFT BLANK

4 Results and Discussion

4.1 Study of the Equations Parameters Used to Obtain the Constant Rates

In this chapter it will be explained how the different parameters of the reaction rate constants equation affects several factors, such as product distribution, O/P ratio and other factors specific to a particular reaction. This information will be important for the latter optimization of the model for the catalytic cracking of small paraffins.

4.1.1 Protolytic Scission

This study began with the protolytic scission reaction, which is considered the initiation step of reaction network since the feed was constituted by a pure small paraffin, n-heptane. The protolytic scission rate constant was calculated using equation 31 adapted from Pinto [57], where k_{0ps} accounts for the intensity of the protolytic scission reaction; a_{ps} relates to the rate of reaction with the reacting paraffin; b_{ps} relates to the rate of reaction with a symmetry criterion. The indexes n and m are the number of carbon atoms of the species involved in this reaction according to equation 1.

$$k_{ps(n,m)} = k_{0ps} \times exp\left(-\left(\frac{a_{ps}}{n} + b_{ps} \times \left(m - \frac{n}{2}\right)^2\right)\right) \quad (31)$$

$$\text{with } 3 \leq \mathrm{n} \leq 20;\ \mathrm{m} \leq \mathrm{n} - 2$$

To study the effect of the different parameters involved in the protolytic scission, each one of them was separately varied with the program, only keeping that single reaction active.

4.1.1.1 Variation of k_{0ps}

The base value of k_{0ps}used in simulations was took as reference of Pinto [1] for the simulation, the order of magnitude was fitted and the value of k_{0ps} was varied 25% and 50%,

positively and negatively. The results obtained for the product distribution when varying this parameter are shown in Figure 10.

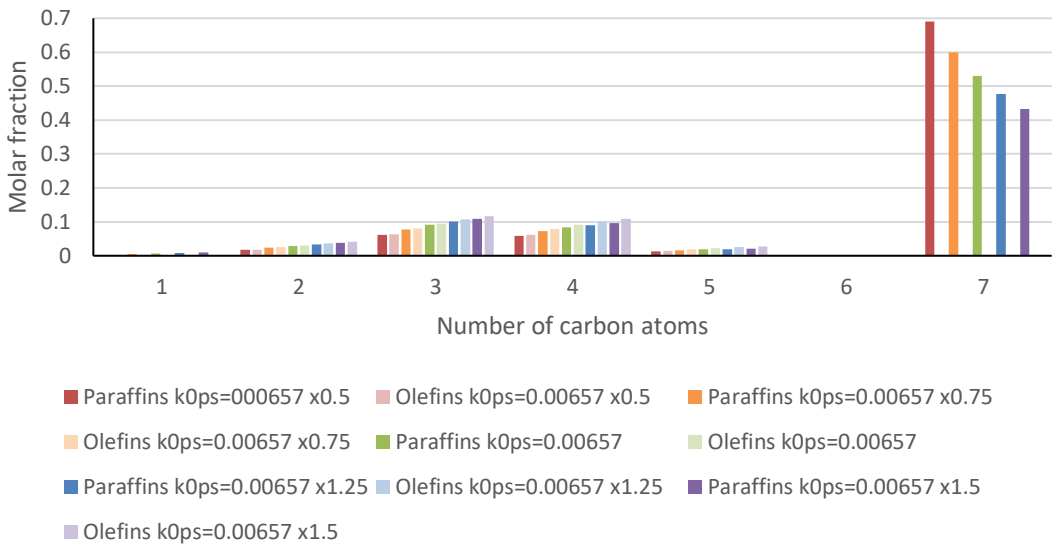

Figure 10 - Reactor outlet stream molar composition for catalytic cracking of n-heptane, using: $a_{ps} = 1.12 \times 10^{1}$, $b_{ps} = 7.04 \times 10^{-1}$ *and varying* k_{0ps}*(mol cm*$^{-3}$ *min*$^{-1}$ *atm*$^{-1}$ *g*$_{cat}$$^{-1}$*).*

As it was expected, k_{0ps} has affected the conversion of the reaction, as can be seen in Figure 10. An increase in the value of k_{0ps} results in an increase in the conversion of the reaction and, consequently, in the molar fraction of all the products.

To properly evaluate the product distribution and quantify the cracking symmetry, the ratio between C_3 plus C_4 and C_2 plus C_5 is evaluated, as shown in Table 1.

Table 1 - Ratio between C_3 *plus* C_4 *and* C_2 *plus* C_5 *variation with* k_{0ps}.

$(C_3+C_4)/(C_2+C_5)$			
k_{0ps}	Paraffin	Olefin	Total
x0.5	3.86	3.75	3.80
x0.75	3.76	3.62	3.69
x1	3.66	3.51	3.58
x1.25	3.57	3.41	3.49
x1.5	3.49	3.32	3.40

Despite an increase on the conversion, the cracking symmetry suffers a minor decrease with the variation of k_{0ps}, as Table 1 presents. The main products remain C_3 and C_4. There is also a minor increase of secondary cracking reactions as can be observed by the O/P ratio small increase presented in Table 2 since the formed paraffins “crack” into smaller ones and the formed olefins accumulate. This also leads to an increase in the formation of methane.

Table 2 - O/P ratio variation with k_{0ps}.

k_{0ps}	O/P Ratio
x0.5	1.03
x0.75	1.05
x1	1.06
x1.25	1.07
x1.5	1.08

4.1.1.2 Variation of a_{ps}

The base value of a_{ps} used in simulations was took as reference of Pinto [1]. For the simulation, the value of a_{ps} was varied 25% and 50%, positively and negatively. The results obtained for the product distribution for this parameter are shown in Figure 11.

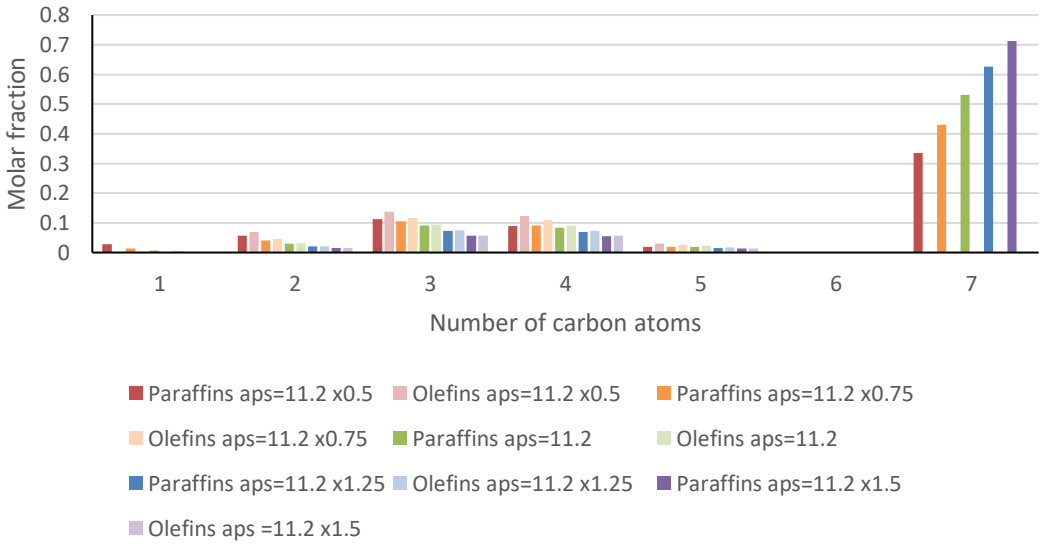

Figure 11 - Reactor outlet stream molar composition for catalytic cracking of n-heptane, using: $k_{0ps} = 6.57 \times 10^{-3}$ mol cm^{-3} min^{-1} atm^{-1} g$_{cat}^{-1}$, $b_{ps} = 7.04 \times 10^{-1}$ and varying a_{ps}.

Similarly to k_{0ps}, a_{ps} also changes the conversion of the reaction. In Figure 11 it can be observed that decreasing the value of a_{ps} increases the conversion of the reaction.

Table 3 - Ratio between C_3 plus C_4 and C_2 plus C_5 variation with a_{ps}.

(C3+C4)/(C2+C5)			
a_{ps}	Paraffin	Olefin	Total
x0.5	2.71	2.60	2.65
x0.75	3.28	3.12	3.19
x1	3.66	3.51	3.58
x1.25	3.88	3.77	3.82
x1.5	3.99	3.92	3.95

However, unlike k_{0ps}, a_{ps} has a more substantial effect in the product distribution, as Table 3 shows. As a_{ps} decreases, the trend to form smaller products (C_1-C_2) increases more than the trend to form C_3-C_5.

The O/P ratio considerably decreases, as it is presented in Table 4. This decrease in this value can be explained by the decrease of the secondary cracking. This occurs when the formed paraffins crack into smaller paraffins and new olefins and these formed olefins accumulate since there are no other reactions considered. Therefore, molar fraction of methane also increases.

Table 4 - O/P ratio variation with a_{ps}.

a_{ps}	O/P Ratio
x0.5	1.19
x0.75	1.11
x1	1.06
x1.25	1.03
x1.5	1.02

4.1.1.3 Variation of b_{ps}

The base value of b_{ps}used in simulations was took as reference of Pinto [1] for simulation, the value of b_{ps} was varied 25% and 50%, positively and negatively. The results obtained for the product distribution variation for this parameter are shown in Figure 12.

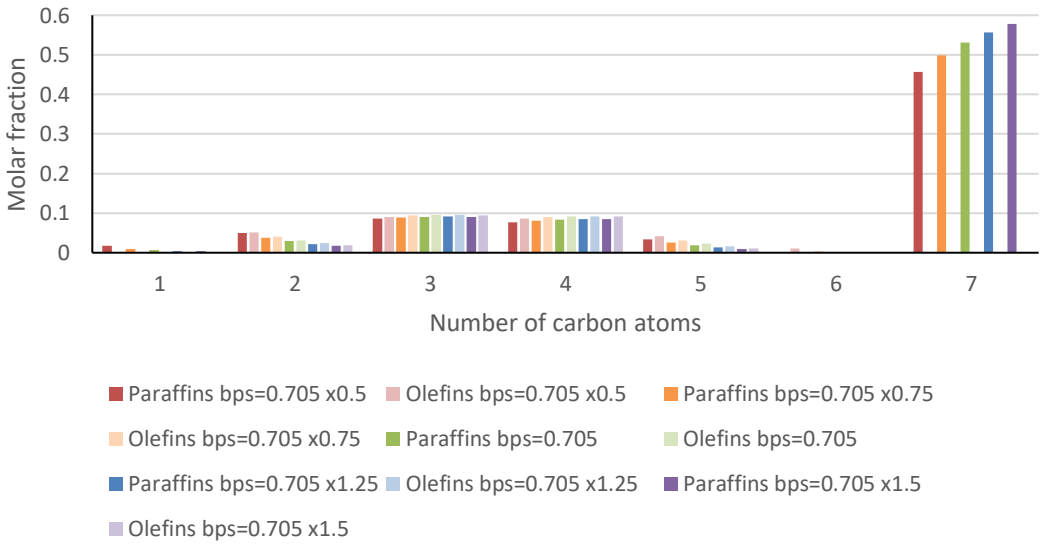

Figure 12 - Reactor outlet stream molar composition for catalytic cracking of n-heptane, using: $k_{0ps} = 6.57 \times 10^{-3}$ mol cm^{-3} min^{-1} atm^{-1} g$_{cat}^{-1}$, $a_{ps} = 1.12 \times 10^{1}$ and varying b_{ps}.

Comparing with the other two parameters previously evaluated),b_{ps} has a slighter effect on the reaction conversion. However, Figure 12 shows that an increase in the value of b_{ps} results in

a decrease of the conversion with a great impact in the product distribution, that can be evaluated in Table 5.

Table 5 - Ratio between C_3 plus C_4 and C_2 plus C_5 variation with b_{ps}.

(C3+C4)/(C2+C5)			
b_{ps}	Paraffin	Olefin	Total
x0.5	1.95	1.90	1.92
x0.75	2.68	2.59	2.63
x1	3.66	3.51	3.58
x1.25	4.95	4.71	4.82
x1.5	6.60	6.21	6.40

Table 5 shows that with the decreasing of b_{ps} value, the product distribution tends to be more uniform. Hence, the molar fraction of the products tends to the same value.

Table 6 - O/P ratio variation with b_{ps}.

b_{ps}	O/P Ratio
x0.5	1.07
x0.75	1.06
x1	1.06
x1.25	1.05
x1.5	1.05

Observing Table 6, it can be noticed that in the reactor outlet stream composition, the O/P ratio increases with the decrease of b_{ps}. This can be easily understood since the product distribution is uniform, as already said. Given that methane comes mainly from the cracking of the reactant into methane and hexene instead of the cracking of the primary cracking paraffins. This can be observed in Figure 12, where methane and hexene molar fractions increase proportionally with the decrease of b_{ps}. The main conclusion to be drawn is that a decrease in the value of b_{ps} results in a decrease in the extension of secondary cracking reactions.

4.1.2 Chain Growth

Due to the nature of the feed, reactions of chain growth have to be evaluated before other reactions because to better understand the influence of hydride transfer, β-scission or even aromatic formation in this complex reaction network, larger olefins must be formed first. The chain growth rate constant was calculated using equation 32 adapted from Pinto [57], where k_{0cg}accounts for the intensity of the chain growth reaction; a_{cg} and b_{cg} relate to the rate of reaction with the reacting olefins. The indexes n and m are the number of carbon atoms of the species involved in this reaction according to equation 2.

$$k_{cg(n,m)} = k_{0cg} \times exp\left(-\left(a_{ps} \times n + \frac{b_{ps}}{m}\right)\right) \qquad (32)$$

$$\text{with } 2 \leq \text{n} \leq 20;\ 2 \leq \text{m} \leq 20$$

In this case, the separate study of the parameters in Equation 32 was performed keeping in the program both protolytic scission and chain growth reactions active. Equation 31 parameter values are presented on Appendix II. It is important to r that hydrocarbons with 21 or more carbon atoms were considered as coke and, thus were not cracked. Thus, coke is formed through chain growth reactions and which are not considered for the calculation of the total outlet flow of the reactor, since it remains adsorbed on surface catalyst after formation and, consequently, do not participate as reactant in any of the reactions considered.

4.1.2.1 Variation of k_{0cg}

The base value of k_{0cg} used in simulations was took as reference of Pinto [1]. For simulation, the order of magnitude was fitted and the value of k_{0cg} was varied 25% and 50%, positively and negatively. The results obtained for this parameter are shown in Figure 13.

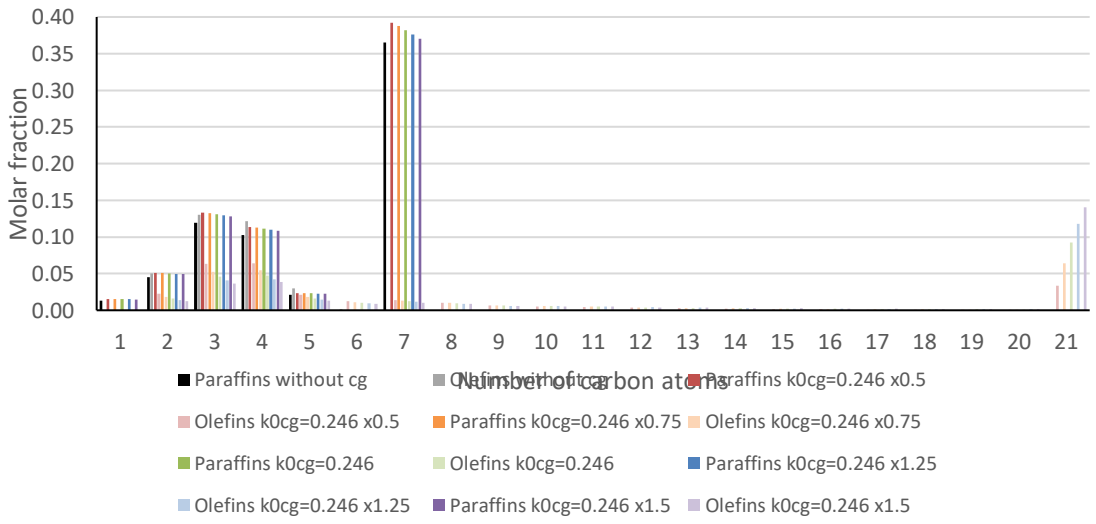

Figure 13 - Reactor outlet stream molar composition for catalytic cracking of n-heptane, using: $a_{cg} = 3.04 \times 10^{-1}$, $b_{cg} = 8.51 \times 10^{-2}$ and varying k_{0cg}(mol cm^{-3} min^{-1} atm^{-2} g$_{cat}^{-1}$).

Figure 13 shows that the inclusion of the chain growth reaction led to appearance of olefins with more than 6 carbon atoms. An increase in value of k_{0cg} also results in an increase in the coke formation. Olefins with 9 or less carbon atoms also decrease. An increase in paraffins molar fractions can also be observed. However this increase does not occur due to an actual increase in the amount of paraffins, since it actually remains constant, but because the total amount of molecules inside the reactor decreases.

Table 7 - O/P ratio variation with k_{0cg}.

k_{0cg}	O/P Ratio
without CG	1.10
x0.5	0.72
x0.75	0.65
x1	0.60
x1.25	0.56
x1.5	0.53

In Table 7 can be observed that increasing the value of k_{0cg} results in a decrease of O/P ratio due to the formation of coke that consumes olefins in an irreversible way. The O/P ratio values with chain growth are considerably lower when compared to the value in absence of chain growth.

4.1.2.2 Variation of a_{cg}

The base value of a_{ps} used in simulations was took as reference of Pinto [1]. For simulation, the value of a_{ps} was varied 25% and 50%, positively and negatively. The results obtained for this parameter are shown in Figure 14.

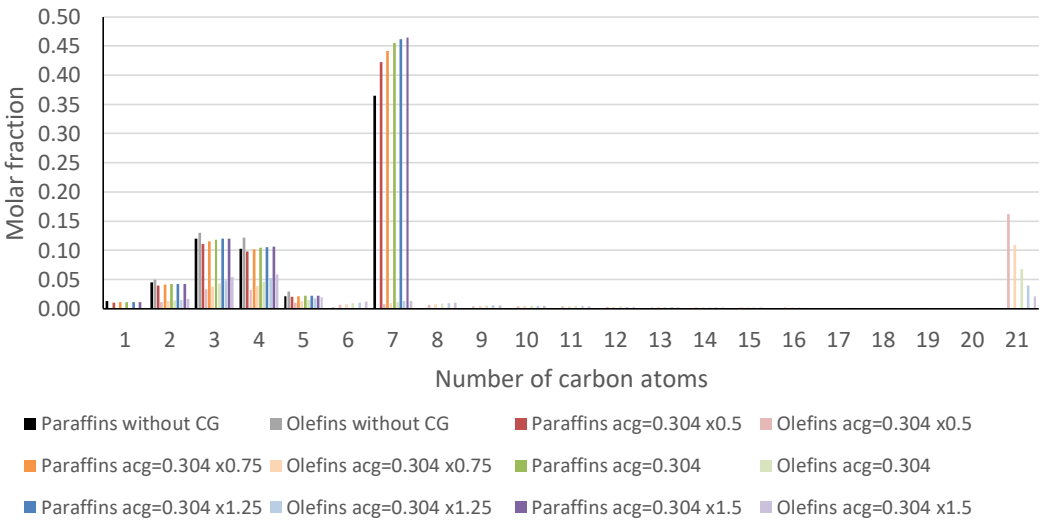

Figure 14 - Reactor outlet stream molar composition for catalytic cracking of n-heptane, using: $k_{0cg} = 2.46 \times 10^{-1}$ mol cm^{-3} min^{-1} atm^{-2} g$_{cat}^{-1}$, $b_{cg} = 8.51 \times 10^{-2}$ and varying a_{cg}.

In Figure 14 can be observed that an increase in value of a_{cg} results in an increase of olefins with less than 10 carbon atoms and a decrease in the formation of olefins with 17 or more carbon atoms as well as coke formation which is also accompanied by an increase of the O/P ratio, as shown in Table 8.

Olefins between 10 and 16 denotes an inversion in the trend with an initial increase followed by a decrease. As the olefin's number of carbon atoms goes up this inflexion in the trend appears at lower values of a_{cg}.

Table 8 - O/P ratio variation with a_{cg}.

a_{cg}	O/P Ratio
without CG	1.10
x0.5	0.49
x0.75	0.55
x1	0.60
x1.25	0.65
x1.5	0.70

4.1.2.3 Variation of b_{cg}

The base value of b_{cg} used in simulations was took as reference of Pinto [1]. For simulation, the order of magnitude was fitted and the value of b_{cg} was varied 25% and 50%, positively and negatively. The results obtained for this parameter are shown in Figure 15.

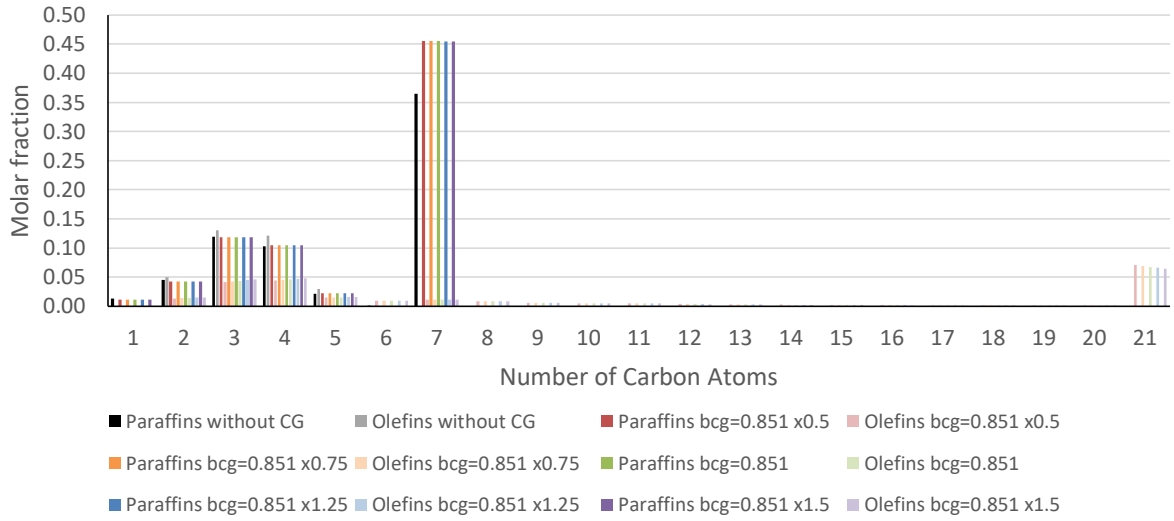

Figure 15 - Reactor outlet stream molar composition for catalytic cracking of n-heptane, using: $k_{0cg} = 2.46 \times 10^{-1}$ mol cm^{-3} min^{-1} atm^{-2} g$_{cat}^{-1}$, $a_{cg} = 3.04 \times 10^{-1}$ and varying b_{cg}.

Comparing with the other two parameters present in equation (4), b_{cg} impact in the extension the chain growth reaction is lower. Figure 15 shows that an increase in b_{cg} results in a mild decrease in the formation of coke.

Table 9 - O/P ratio variation with b_{cg}.

b_{cg}	O/P Ratio
without CG	1.10
x0.5	0.59
x0.75	0.60
x1	0.60
x1.25	0.61
x1.5	0.62

As expected, Table 9 shows that b_{cg} variation has a minimal repercussion in the O/P ratio.

4.1.3 Hydride Transfer

The next step of this study is the inclusion of hydride transfer reactions. Since there is now a wide range of olefins, due to the chain growth reactions, one are allowed to more deeply understand which paraffins and olefins tend to be formed and consumed through this reaction. The hydride transfer rate constant was calculated using equation 33 adapted from Pinto [57], where k_{0ht} accounts for the intensity of the hydride transfer reaction; a_{ht} and b_{ht} relates to the rate of reaction with the reacting olefins and paraffins, respectively The indexes n and m are the number of carbon atoms of the species involved in this reaction according to equation 3.

$$k_{ht(n,m)} = k_{0ht} \times exp\left(-\left(a_{ht} \times n + \frac{b_{ht}}{m}\right)\right) \quad (33)$$

$$\text{with } 2 \leq \text{n} \leq 20;\ 2 \leq \text{m} \leq 20$$

For this situation, the study of the separated parameters that appear in Equation 33 was performed keeping active in the program all the reactions previously studied and hydride transfer reactions. Equations 31 and 32 parameter values are presented on Appendix II.

4.1.3.1 Variation of k_{0ht}

To study the effect of k_{0ht} the value of Pinto [1] was took as reference. The order of magnitude was fitted and variations of 25% and 50% were performed, as in the previous simulations. The results obtained for this parameter are shown in Figure 16.

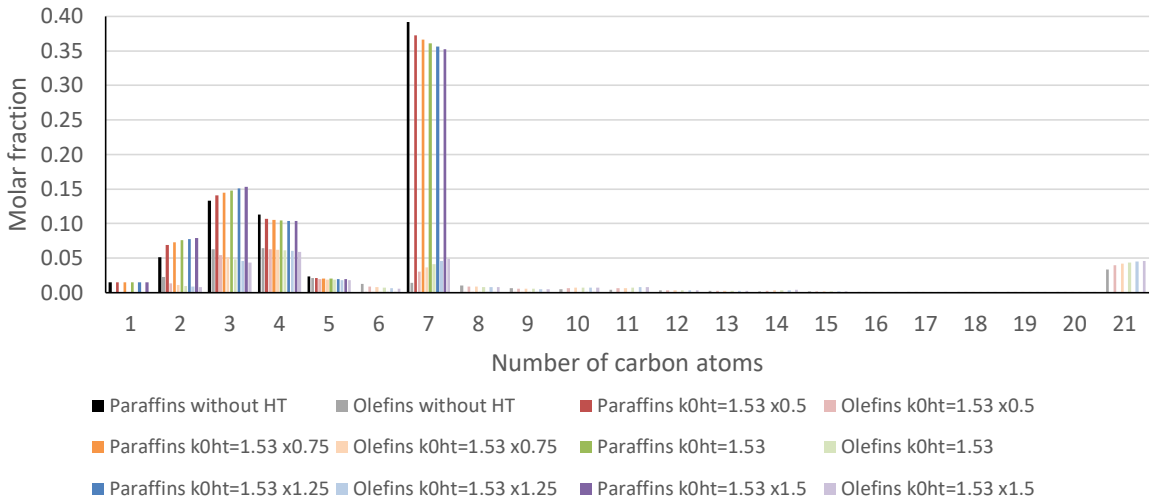

Figure 16 - Reactor outlet stream molar composition for catalytic cracking of n-heptane, using: $a_{ht} = 1.41 \times 10^{0}$, $b_{ht} = 1.78 \times 10^{-1}$ *and varying* k_{0ht}*(mol cm^{-3} min^{-1} atm^{-2} g$_{cat}^{-1}$).*

Figure 16 shows that an increase in value of k_{0ht} results in a decrease in the molar fraction of smaller olefins between 2 and 5 carbon atoms while the molar fraction of heptene increases. There is also a slight increase on coke formation. In Figure 16 it can also be observed that an increase in value of k_{0ht} results in an increase in the molar fraction of ethane and propane. Unexpectedly, butane and pentane molar fractions denotes a slight decrease. Heptane's molar fraction also decreases. Also occurs the formation of paraffins with more than 7 carbon atoms which did not occur prior to the implementation of the hydride transfer reaction in the model.

To quantify the extension of hydride transfer reaction the ratio between propane and propylene was used, because these species are among the main products in the catalytic cracking of n-heptane and are easy to quantify experimentally since they do not have isomers.

Table 10 - Ratio between propane and propylene variation with k_{0ht}.

k_{0ht}	P_3/O_3 Ratio
Without HT	2.10
x0.5	2.57
x0.75	2.82
x1	3.06
x1.25	3.30
x1.5	3.53

Table 10 shows that P_3/O_3 ratio increases with the increase of k_{0ht} value. While comparing these values with the P_3/O_3 ratio value without the hydride transfer reaction, it can be concluded that increasing the k_{0ht} value increases the extension of the hydride transfer reaction since the P_3/O_3 ratio value diverges from the value where this reaction is not implemented.

Table 11 - O/P ratio variation with k_{0ht}.

k_{0ht}	O/P Ratio
Without HT	0.71
x0.5	0.66
x0.75	0.65
x1	0.64
x1.25	0.63
x1.5	0.62

Table 11 shows a slight decrease of the O/P ratio when the hydride transfer reaction is implemented. O/P ratio gets lower while the k_{0ht} value increase which is related to a slight increase on the coke formation.

4.1.3.2 Variation of a_{ht}

To study the effect of a_{ht} the value of Pinto [1] was took as reference and has undergone variations, positive and negative, of 25% and 50%. The results obtained for this parameter are shown in Figure 17.

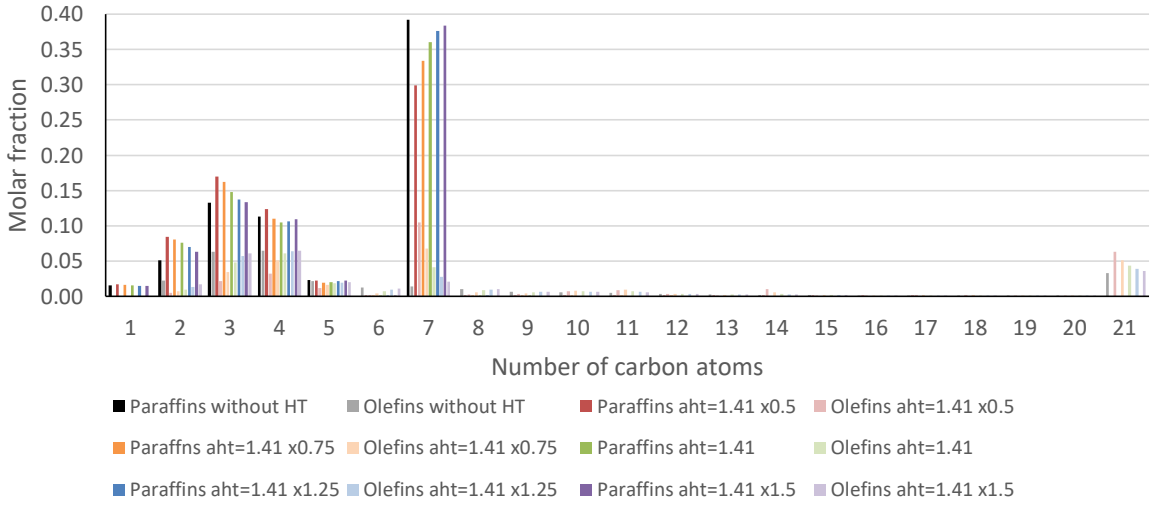

Figure 17 - Reactor outlet stream molar composition for catalytic cracking of n-heptane, using: $k_{0ht} = 1.53 \times 10^{0}$ mol cm^{-3} min^{-1} atm^{-2} g$_{cat}^{-1}$, $b_{ht} = 1.78 \times 10^{-1}$ and varying a_{ht}.

Contrarily to k_{0ht}, an increase in a_{ht} value results in an increase in heptane molar fraction and a decrease in the molar fraction of C_2-C_3 paraffins, as shown in Figure 17. However, in the molar fractions of butane and pentane there is an inversion in the trend. For a_{ht} values below the reference value, the molar fraction of butane tends to decrease with the increase of a_{ht} value. For a_{ht} values above the reference value, the molar fraction of butane increase tends to increase with value. In pentane molar fraction this point of inversion appears at a negative variation of 25% of the reference value. Olefins between 2 and 6 number of carbon atoms, this inflection does not exist. Their molar fractions just increase while increasing a_{ht} value.

Table 12 - Ratio between propane and propylene variation with a_{ht}.

a_{ht}	P_3/O_3 Ratio
Without HT	2.10
x0.5	7.89
x0.75	4.68
x1	3.06
x1.25	2.41
x1.5	2.18

Table 12 presents a decrease in P_3/O_3 ratio with the increase of a_{ht} value, due to the simultaneous decrease of propane and increase of propylene molar fractions. While comparing these values with the one of the simulation where hydride transfer does not exist, it can be concluded that increasing the a_{ht} value decreases the extension of the hydride transfer reaction since the P_3/O_3 ratio value converges to the value where this reaction is not considered. Through the analysis of these facts it can be concluded that this parameter not only affects the extension of this reaction, but also controls the number of carbon atoms in which the trends of paraffins are reversed.~

Table 13 - O/P ratio variation with a_{ht}.

a_{ht}	O/P Ratio
Without HT	0.71
x0.5	0.53
x0.75	0.58
x1	0.64
x1.25	0.67
x1.5	0.69

In Table 13 can be observed that there is a slight increase in the O/P ratio. This occurs, not only, due to the decrease of light paraffins molar fractions, but also, due to the increase of light olefins. Like the P_3/O_3 ratio, the O/P ratio also tends to value of the simulation where the hydride transfer is not considered with the increase of a_{ht} which can be concluded that increasing too much the a_{ht} value cancels the hydride transfer.

4.1.3.3 Variation of b_{ht}

To study the effect of b_{ht} the value of Pinto [1] was took as reference and has undergone variations, positive and negative, of 25% and 50%. The results obtained for the variations in this parameter are shown in Figure 18.

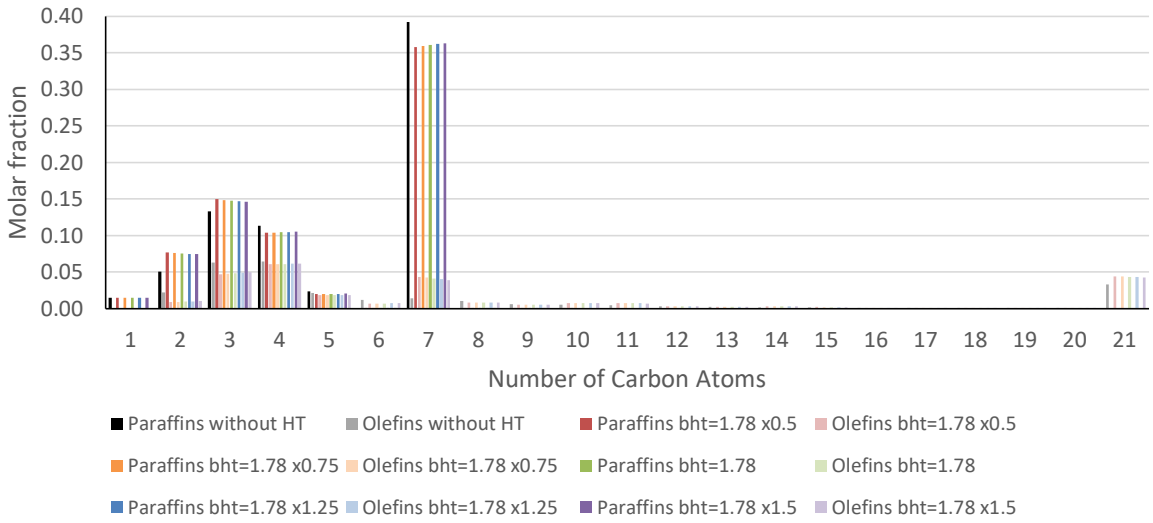

Figure 18 - Reactor outlet stream molar composition for catalytic cracking of n-heptane, using: $k_{0ht} = 1.53 \times 10^0$ *mol cm*$^{-3}$ *min*$^{-1}$ *atm*$^{-2}$ g_{cat}^{-1}, $a_{ht} = 1.41 \times 10^0$ *and varying* b_{ht}.

Unlike the two previous parameters, b_{ht} has a minimal effect in this reaction extension. In Figure 18 can be observed that ethane and propane molar fractions decrease while the molar fractions of butane and pentane increase. Also, the molar fractions of olefins between 2 and 6 atoms of carbon increase. Heptene molar fraction decreases while heptane's increases meaning that the conversion decreases.

The effect of b_{ht} in the extension of the hydride transfer reaction can also be observed in Table 14. An increase in b_{ht} results in a mild decrease in the P_3/O_3 ratio. Similarly to a_{ht}, an increase in b_{ht} value results in a decreases the extension of the hydride transfer reaction once the P_3/O_3 ratio value converges to the one when hydride transfer is not implemented.

Table 14 - Ratio between propane and propylene variation with b_{ht}.

b_{ht}	P_3/O_3 Ratio
Without HT	2.10
x0.5	3.20
x0.75	3.12
x1	3.06
x1.25	3.00
x1.5	2.94

Since the variation of b_{ht} has a minimal impact in extension of the reaction, the same happens with the O/P ratio as shown in Table 15. However a small decrease is observed. Increasing too much this parameter also tends to cancel the hydride transfer reactions.

Table 15 - O/P ratio variation with b_{ht}.

b_{ht}	O/P Ratio
Without HT	0.71
x0.5	0.63
x0.75	0.64
x1	0.64
x1.25	0.64
x1.5	0.64

These facts points to the conclusion that the hydride transfer reaction is mainly influenced by the reactant olefin. However this can be related to equation used for the calculation of the constant rates since the model from Pinto [1] accounts the carbenium ions and this model do not.

4.1.4 β-Scission

Another important reaction to be studied is the β-scission. The β-scission rate constant was calculated using equation 34 adapted from Pinto [57], where k_{0bs} accounts for the intensity of the β-scission reaction; a_{bs} relates the rate of reaction with the reacting olefin and b_{bs} relates the rate of reaction with one of the formed olefins. The indexes n and m are the number of carbon atoms of the species involved in this reaction according to equation 4.

$$k_{bs(n,m)} = k_{0bs} \times exp\left(-\left(\frac{a_{bs}}{n} + \frac{b_{bs}}{m}\right)\right) \qquad (34)$$

$$\text{with } 5 \leq \text{n} \leq 20;\ 2 \leq \text{m} \leq 18$$

To study the effect of each parameter involved in the β-scission reaction, the program was run with protolytic, chain growth and β-scission reactions active, varying, separately, each parameter of equation 34. Equations 31-33 parameter values are presented on Appendix II.

4.1.4.1 Variation of k_{0bs}

The value of k_{0bs} used in simulations was took as reference of Pinto [1]. For the simulation, the order of magnitude was changed in relation to the value in [1] and the value of k_{0bs} was varied 25% and 50%, positively and negatively. The results obtained for this parameter are shown in Figure 19.

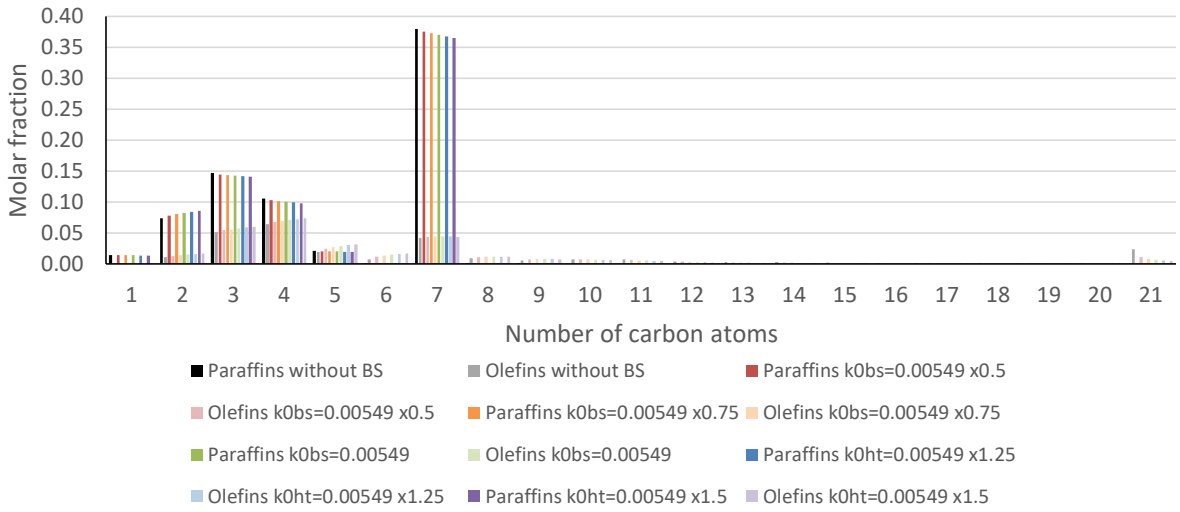

Figure 19 - Reactor outlet stream molar composition for catalytic cracking of n-heptane, using: $a_{bs} = 1.11 \times 10^{1}$, $b_{bs} = 1.59 \times 10^{0}$ *and varying* k_{0bs}*(mol cm*$^{-3}$ *min*$^{-1}$ *atm*$^{-1}$ g_{cat}^{-1}*).*

It can be observed in Figure 19 that the implementation of β-scission reaction produces an increase in the lighter olefins molar fractions. Increasing k_{0bs} results in an increase of olefins' molar fractions from 2 to 6 carbon atoms and a decrease in olefins' molar fractions between 10 and 20 carbon atoms. Olefins' molar fractions with 7 to 9 carbon atoms present an inversion. This happens because at some point the cracking rates of these olefins get bigger than their formation rates. There is also an indirect decrease of coke's molar fraction through the cracking of heavier olefins preventing them from transforming into coke through the chain growth reaction.

Table 16 - O/P ratio variation with k_{0bs}*.*

k_{0bs}	O/P Ratio
without BS	0.72
x0.5	0.74
x0.75	0.75
x1	0.76
x1.25	0.77
x1.5	0.78

As shown in Table 16 the β-scission, which corresponds to secondary cracking reaction of olefins, promotes a slight increase of the O/P ratio due to the formation of more olefins and the decrease of coke formation.

4.1.4.2 Variation of a_{bs}

To study the effect of a_{bs} the value of Pinto [1] was took as reference and has undergone variations, positive and negative, of 25% and 50%. The results obtained for this parameter are shown in Figure 20.

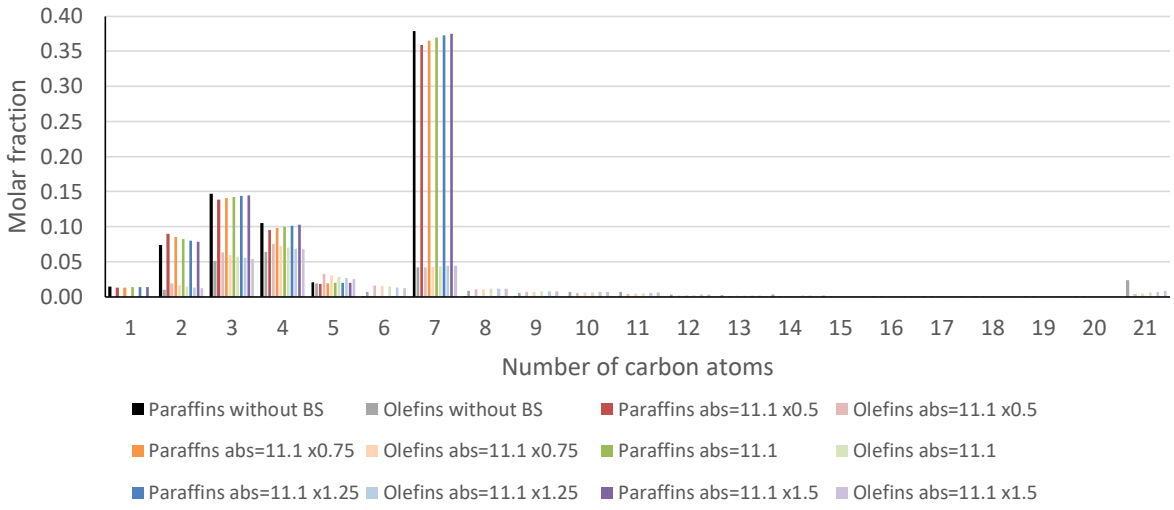

Figure 20 - Reactor outlet stream molar composition for catalytic cracking of n-heptane, using: $k_{0bs} = 5.49 \times 10^{-3}$ *mol cm*$^{-3}$ *min*$^{-1}$ *atm*$^{-1}$ *g*$_{cat}^{-1}$, $b_{bs} = 1.59 \times 10^{0}$ *and varying* a_{bs}.

Increasing a_{bs} reduces the β-scission extension, as presented in Figure 20. While increasing a_{bs}, there is an increase in olefins' molar fractions between 2 and 6 carbons, a decrease with 7 and from 9 to 20 carbon atoms and an inversion with 8 carbon atoms. There is also an indirect increase in coke formation.

Table 17 - O/P ratio variation with a_{bs}.

a_{bs}	O/P Ratio
without BS	0.72
x0.5	0.80
x0.75	0.78
x1	0.76
x1.25	0.75
x1.5	0.74

Again, in contrast with k_{bs}^{0}, there is a slight decrease of the O/P ratio with the increase of a_{bs}, since there are less olefins formed and the coke formation increased. This can be observed in Table 17.

4.1.4.3 Variation of b_{bs}

To study the effect of b_{bs} the value of Pinto [1] was took as reference and has undergone variations, positive and negative, of 25% and 50%. The results obtained for this parameter are shown in Figure 21.

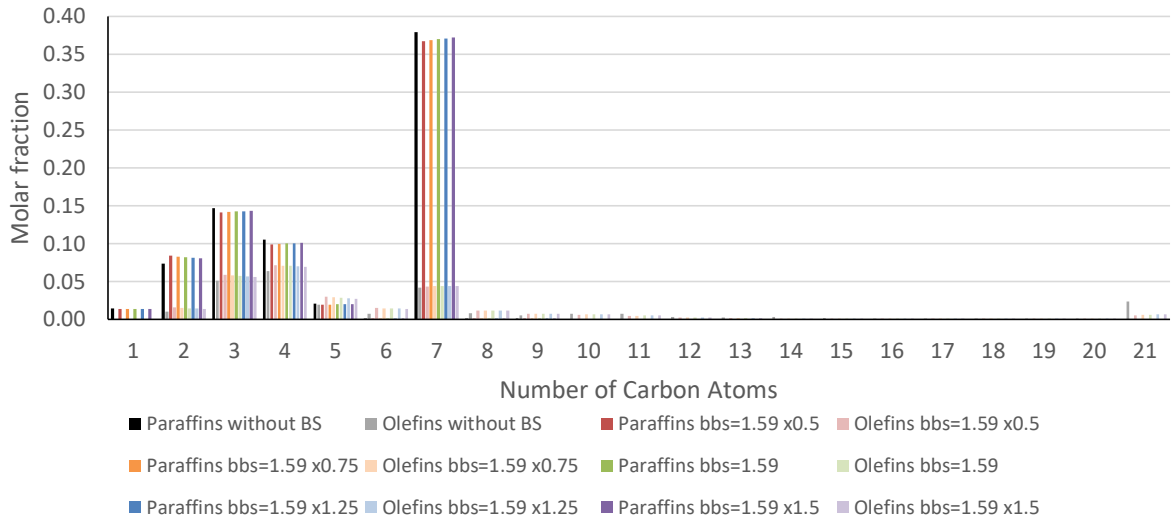

Figure 21 - Reactor outlet stream molar composition for catalytic cracking of n-heptane, using: $k_{0bs} = 5.49 \times 10^{-3}$ *mol cm*$^{-3}$ *min*$^{-1}$ *atm*$^{-1}$ *ng*$_{cat}^{-1}$, $a_{bs} = 1.11 \times 10^{1}$ *and varying* b_{bs}.

Figure 21 shows that an increase in b_{bs} results in decrease olefins' molar fraction between 2 and 6 carbon atoms and an increase from 7 to 20 carbon atoms. There is also an indirect increase in coke formation. However, these variations are slighter than the ones observed with the variation of a_{bs}.

Table 18 - O/P ratio variation with b_{bs}.

b_{bs}	O/P Ratio
without BS	0.72
x0.5	0.77
x0.75	0.77
x1	0.76
x1.25	0.76
x1.5	0.75

Since the increasing of b_{bs} value produce the almost the same variation as a_{bs} but with a slighter effect, the O/P ratio also presents decrease, but even less significant than the one observed with a_{bs}, as presented in Table 18.

4.1.5 Aromatic Formation

Another reaction to be studied, because it is relevant in the overview of cracking process, despite the fact that if occurs in much less extent, is the aromatic formation. The aromatic formation rate constant was calculated using equation 35. Unlike the previous equations used to calculate constant rates of reaction, this equation is not from Pinto [57]. It has a pre-exponential factor, $k_{0ar(m)}$, related to intensity of the aromatic formation reaction and since were only considered aromatics between 6 and 8 carbon atoms there is a different value of k_{0ar} for each

value of m, which did not happen in the previous reactions. It also has a parameter in the exponential, a_{ar}, which relates to the reacting olefins that will form paraffins, which is similar to a_{ht} from the hydride transfer reaction. The indexes n and m are the number of carbon atoms of the species involved in this reaction according to equation 5.

$$k_{ar(n,m)} = k_{0ar(m)} \times exp(-a_{ar} \times n) \quad (35)$$
$$\text{with } 2 \leq n \leq 20;\ 6 \leq m \leq 8$$

To study the effect of each parameter involved in the aromatic formation reaction, the program was run with all the previous reactions active, varying, separately, each parameter of equation 35. Equations 31-34 parameter values are presented on Appendix II.

4.1.5.1 Variation of $k_{0ar(6)}$

To study the effect of $k_{0ar(6)}$ the value of Pinto [1] was took as reference. The order of magnitude was fitted and variations of 25% and 50% were performed, as in the previous simulations. The results obtained for this parameter are shown in Figure 22.

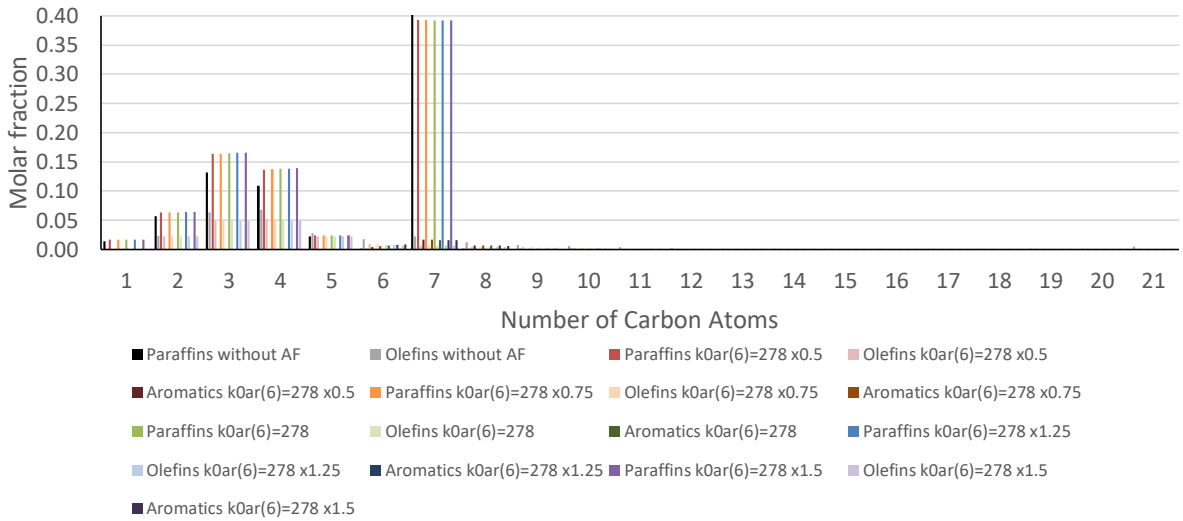

Figure 22 - Reactor outlet stream molar composition for catalytic cracking of n-heptane, using: $k_{0ar(7)} = 8.01 \times 10^2$ *mol cm*$^{-3}$ *min*$^{-1}$ *atm*$^{-4}$ g_{cat}^{-1}, $k_{0ar(8)} = 5.85 \times 10^2$ *mol cm*$^{-3}$ *min*$^{-1}$ *atm*$^{-4}$ g_{cat}^{-1}, $a_{ar} = 1.41 \times 10^{-1}$ *and varying* $k_{0ar(6)}$*(mol cm*$^{-3}$ *min*$^{-1}$ *atm*$^{-4}$ g_{cat}^{-1}*).*

In Figure 22 can be seen that inclusion of the aromatic formation, despite the fact that this reaction is somewhat residual, its effect in the production of paraffins and the consumption of olefins cannot be neglected. However, the variation of its parameters produces only very slight variations in the product distribution, as it will be seen across this study. Nevertheless, while increasing $k_{0ar(6)}$ there is an increase in benzene's molar fraction. The major increases in paraffin

molar fractions are in propane's and butane's while the major decreases in olefin molar fractions are in propylene, butene and, of course, hexene.

Table 19 - O/P ratio variation with $k_{0ar(6)}$.

$k_{0ar(6)}$	O/P Ratio
without AF	0.78
x0.5	0.43
x0.75	0.43
x1	0.42
x1.25	0.41
x1.5	0.41

As expected, it can be seen in Table 19 that there is a minimal decrease in the O/P ratio since variations in the product distribution are only residual. However, while comparing the O/P ratio value with and without the aromatics formation, there is a huge decrease in the O/P ratio value which proves the importance of this reaction in paraffins formation and olefins consumption.

4.1.5.2 Variation of $k_{0ar(7)}$

To study the effect of $k_{0ar(7)}$ the value of Pinto [1] was took as reference. The order of magnitude was fitted and variations of 25% and 50% were performed, as in the previous simulations. The results obtained for this parameter are shown in Figure 23.

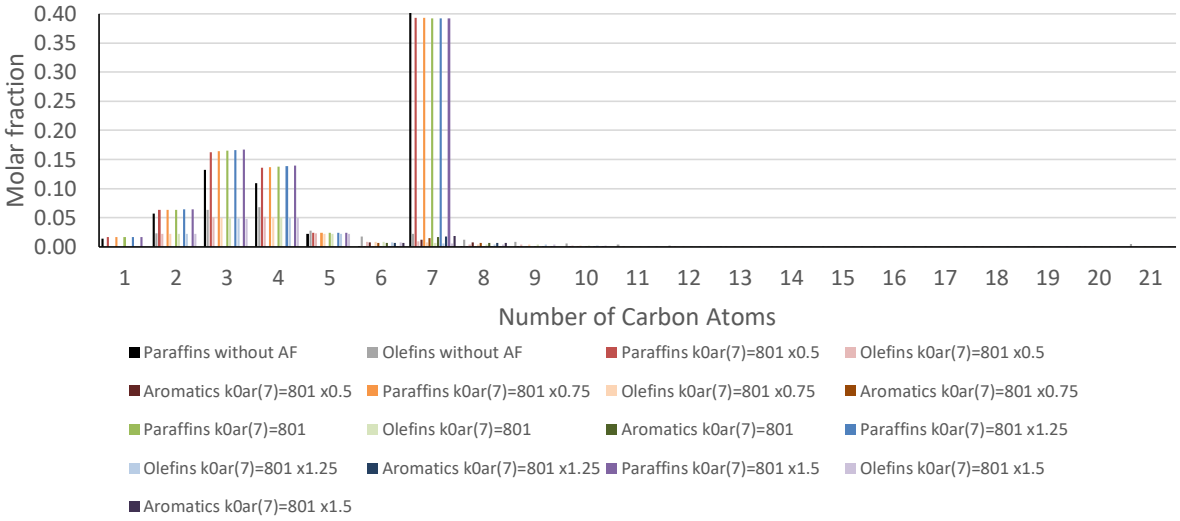

Figure 23 - Reactor outlet stream molar composition for catalytic cracking of n-heptane, using: $k_{0ar(6)} = 2.78 \times 10^2$ mol cm^{-3} min^{-1} atm^{-4} g$_{cat}^{-1}$,$k_{0ar(8)} = 5.85 \times 10^2$ mol cm^{-3} min^{-1} atm^{-4} g$_{cat}^{-1}$, $a_{ar} = 1.41 \times 10^{-1}$ and varying $k_{0ar(7)}$(mol cm^{-3} min^{-1} atm^{-4} g$_{cat}^{-1}$).

Similarly to $k_{0ar(7)}$ the variations in the product distribution obtain with the variation of $k_{0ar(7)}$ are minimal, as presented in Figure 23. While increasing $k_{0ar(7)}$ there is an increase in toluene's

molar fraction. The major increases in paraffin fractions are in propane's and butane's while the major decreases in olefin molar fractions are in propylene, butene and, of course, heptene.

Table 20 - O/P ratio variation with $k_{0ar(7)}$.

$k_{0ar(7)}$	O/P Ratio
without AF	0.78
x0.5	0.45
x0.75	0.43
x1	0.42
x1.25	0.41
x1.5	0.41

Table 20 shows that the variations in the O/P ratio, again, are minimal when $k_{0ar(7)}$ is varied, however the decrease in the O/P ratio is a slightly bigger, while comparing with the previous parameter, because the variations in the product distribution are also a bit bigger.

4.1.5.3 Variation of $k_{0ar(8)}$

To study the effect of $k_{0ar(8)}$ the value of Pinto [1] was took as reference. The order of magnitude was fitted and variations of 25% and 50% were performed, as in the previous simulations. The results obtained for this parameter are shown in Figure 24.

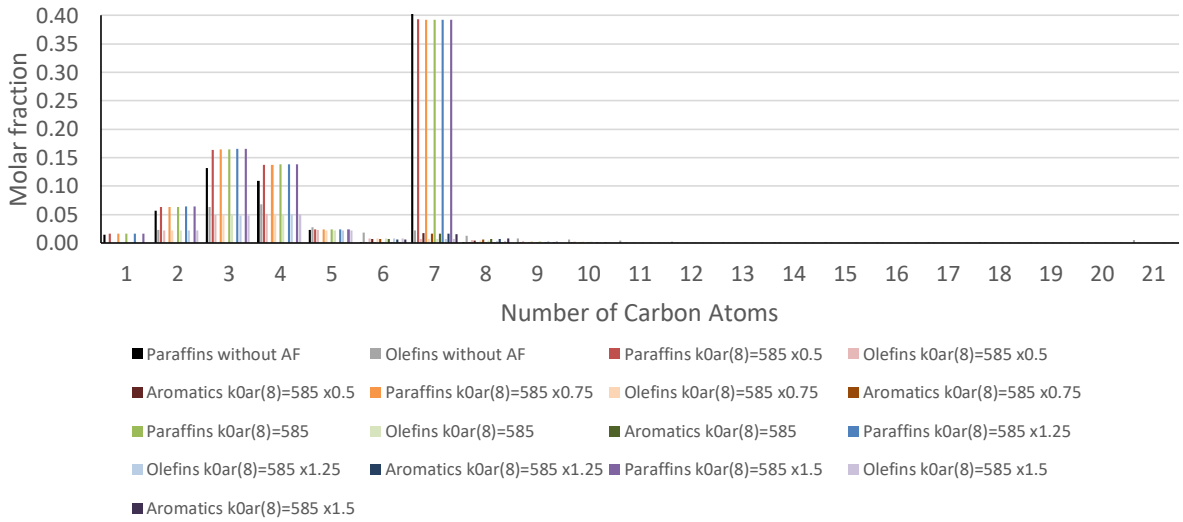

Figure 24 - Reactor outlet stream molar composition for catalytic cracking of n-heptane, using: $k_{0ar(6)} = 2.78 \times 10^2$ mol cm^{-3} min^{-1} atm^{-4} g$_{cat}^{-1}$,$k_{0ar(7)} = 8.01 \times 10^2$ mol cm^{-3} min^{-1} atm^{-4} g$_{cat}^{-1}$, $a_{ar} = 1.41 \times 10^{-1}$ and varying $k_{0ar(8)}$ (mol cm^{-3} min^{-1} atm^{-4} g$_{cat}^{-1}$).

Like the two previous parameters, the variations obtained in the product distribution from $k_{0ar(8)}$ are small, as presented in Figure 24. An increase $k_{0ar(8)}$ results in an increase of xylene's and ethyl-benzene's molar fractions. The major increases in paraffin molar fractions are in

propane's and butane's while the major decreases in olefin molar fractions are in propylene, butene and, of course, octene.

Table 21 - O/P ratio variation with $k_{0ar(8)}$.

$k_{0ar(8)}$	O/P Ratio
without AF	0.78
x0.5	0.43
x0.75	0.42
x1	0.42
x1.25	0.42
x1.5	0.41

As shown in Table 21, the variation in the O/P ratio with $k_{0ar(8)}$ are minimal and at the same level as the one obtained for $k_{0ar(6)}$ however there are less olefins with 8 carbon atoms to form aromatics than with 6.

4.1.5.4 Variation of a_{ar}

To study the effect of a_{ar} the value of a_{ht} was took as reference. The order of magnitude was fitted and variations of 25% and 50% were performed. The results obtained for this parameter are shown in Figure 25.

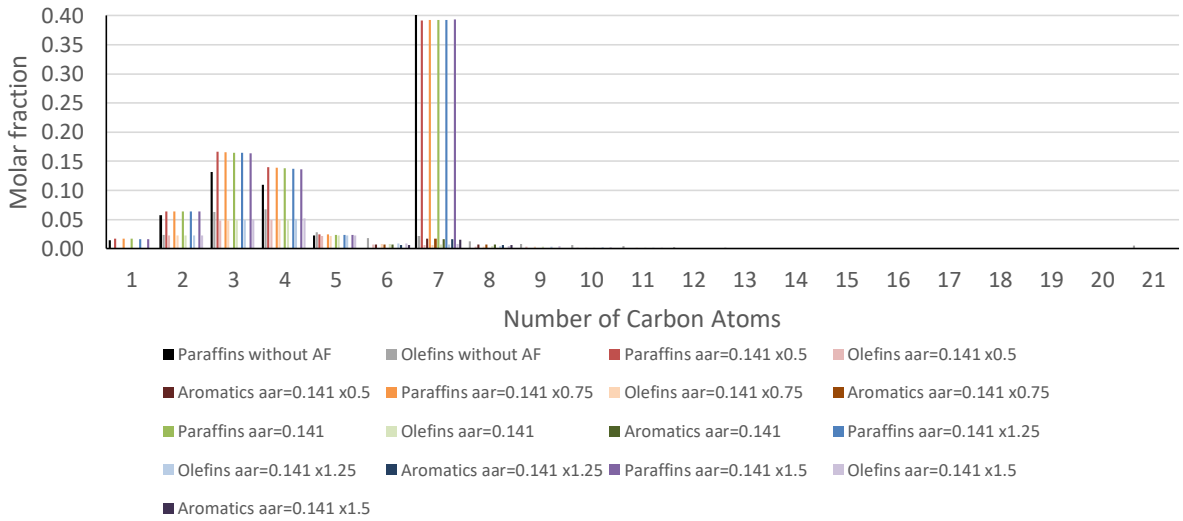

Figure 25 - Reactor outlet stream molar composition for catalytic cracking of n-heptane, using: $k_{0ar(6)} = 2.78 \times 10^2$ mol cm^{-3} min^{-1} atm^{-4} g$_{cat}^{-1}$, $k_{0ar(7)} = 8.01 \times 10^2$ mol cm^{-3} min^{-1} atm^{-4} g$_{cat}^{-1}$, $k_{0ar(8)} = 5.85 \times 10^2$ mol cm^{-3} min^{-1} atm^{-4} g$_{cat}^{-1}$, and varying a_a.

Unlike the previous parameters, the extension of aromatic formation reaction decreases while increasing a_{ar}, as shown in Figure 25. While increasing a_{ar} there is a general increase of olefins molar fractions, having the major increases olefins with 3 and 4 and between 6 and 8

carbon atoms. There is also a decrease in all aromatics molar fractions and a general decrease in paraffins molar fractions with major ones being propane and butane.

Table 22 - O/P ratio variation with a_{ar}.

a_{ar}	O/P Ratio
without AF	0.78
x0.5	0.40
x0.75	0.41
x1	0.42
x1.25	0.43
x1.5	0.44

Contrasting with the previous parameters, Table 22 shows that there is a decrease in the O/P ratio while increasing a_{ar}. This occurs mainly because there is a general decrease in reaction rates of aromatic formation and less olefins are being transformed into paraffins and aromatics.

4.1.6 Paraffins Isomerization

The last reaction to be studied is the paraffins isomerization. The forward rate constant, was calculated using an exponential function (39), with a pre-exponential factor, k_{0iso}, related to the intensity of the forward reaction; and a parameter in exponential, a_{iso}, related with the reacting linear paraffin. The index n are the number of carbon atoms of the species involved in this reaction according to equation 6.

$$k_{iso(n)} = k_{0iso} \times exp(-a_{iso} \times n) \qquad (39)$$
$$\text{with } 4 \leq \text{m} \leq 20$$

The final equation used to calculate the isomerization elementary step reaction rate is defined by equation 40.

$$r_{iso(n)} = k_{0iso} \times exp(-a_{iso} \times n) \times \left(P_{nP_n} - \frac{P_{iP_n}}{0.0284 \times exp(0.901 \times n)}\right) \times w \qquad (40)$$
$$\text{with } 4 \leq \text{n} \leq 20$$

To study the effect of each parameter involved in the isomerization reaction, the program was run with all the previous reactions active, varying, separately, each parameter of equation (40). Equations 31-35 parameter values are presented on Appendix II.

In this stage of the study only linear and branched paraffins are represented since olefins and aromatics molar fractions does not change with the variations implemented.

4.1.6.1 Variation of k_{0iso}

To study the effect of k_{0iso} several values were tested and the results were compared with the experimental results. Then, variations of 25% and 50% were performed, as in the previous simulations. The results obtained for this parameter are shown in Figure 26.

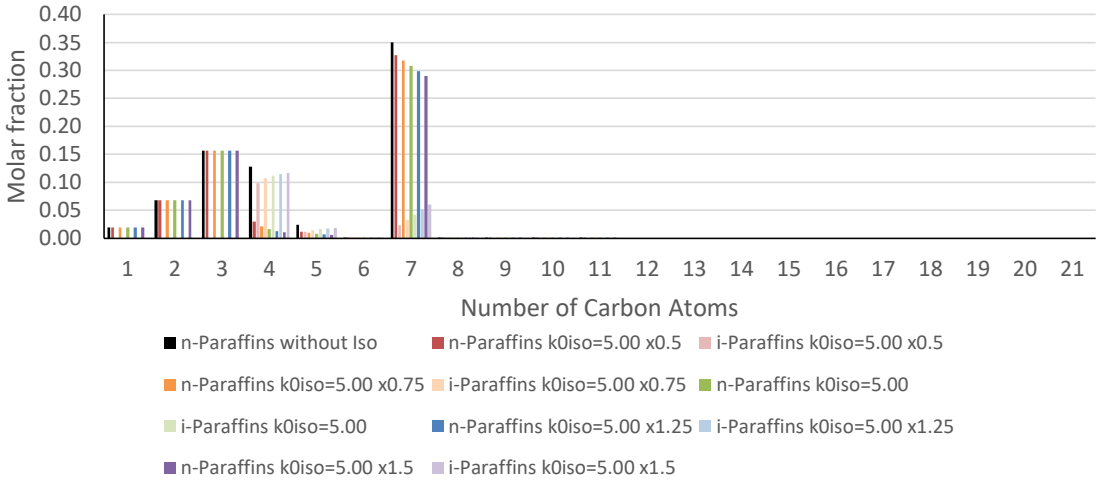

Figure 26 - Reactor outlet stream molar composition for catalytic cracking of n-heptane, using: $a_{iso} = 1.12 \times 10^0$ *and varying* k_{0sio}*(mol cm^{-3} min^{-1} atm^{-1} g$_{cat}^{-1}$).*

In Figure 26 can be observed that molar fraction of paraffins with less than 4 carbon atoms do not suffer any variation since they do not have any isomer. Also, the extension of isomerization reaction increases while k_{0iso} increases. There is a general increase of branched paraffins molar fractions and general decrease of linear paraffins molar fractions as k_{0iso} increases.

Table 23 - O/P ratio variation with k_{0iso}.

k_{0iso}	O/P Ratio
without Iso	0.61
x0.5	0.58
x0.75	0.57
x1	0.55
x1.25	0.54
x1.5	0.53

Since the total amount of paraffin and olefin molecules remain constant inside the reactor the O/P ratio should remain constant too. However, this is not verified as can be observed in Table 23. This variation on O/P ratio occurs because the reactant is not accounted in the O/P ratio value. Despite the total amount of paraffin molecules inside the reactor remains constant, the amount of paraffins which are accounted for the calculation of O/P ratio does not remain. N-heptane reacts through isomerization and forms branched paraffins with 7 carbon atoms

increasing the amount of paraffins which are accounted for the calculation of O/P ratio hence decreasing its value.

4.1.6.2 Variation of a_{iso}

To study the effect of a_{iso} the value of a_{ps} was took as reference. The order of magnitude was fitted and variations of 10% and 20% were performed. The results obtained for this parameter are shown in **Error! Reference source not found.**.

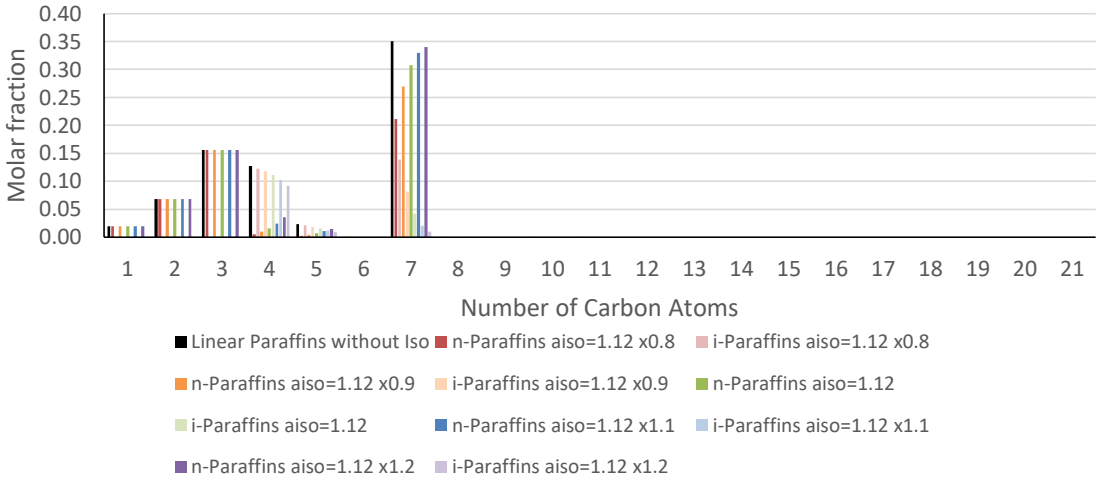

Figure 27 - Reactor outlet stream molar composition for catalytic cracking of n-heptane, using: $k_{0iso} = 8.00 \times 10^0$ *mol cm*$^{-3}$ *min*$^{-1}$ *atm*$^{-1}$ *g*$_{cat}^{-1}$ *and varying* a_{iso}.

Figure 27 shows that a_{iso} has a huge impact in the extension of the isomerization reaction. As a_{iso} increases linear paraffins molar fractions increases and branched paraffins molar fractions decreases. Also, the variations caused by this parameter will be higher of higher number of carbon atoms.

Table 24 - O/P ratio variation with a_{iso}.

a_{iso}	O/P Ratio
without Iso	0.61
x0.8	0.45
x0.9	0.51
x1	0.55
x1.1	0.58
x1.2	0.60

The variations in the O/P ratio observed for a_{iso}, as shown in Table 24, are much more significant than the ones verified for k_{iso}^0 because the variation of n-heptane molar fraction is much higher.

4.2 Fitting Model to Experimental Data

The model was fitted to the experimental data obtain by Borges [58] for n-heptane, through the variation of the set of parameters used to calculate the rate constants using a reactant partial pressure of 0.42 atm. The parameters value set were varied manually. The final parameters value set that would be used in every simulation to test the model applicability are presented in Table 25. The results of the model's fit to the experimental data of n-heptane are presented Figure 28.

Table 25 - Set of parameters used to fit the model to experimental data.

Parameter	Value
k_{0ps} (mol cm^{-3} min^{-1} atm^{-1} g$_{cat}^{-1}$)	1.10×10^{-2}
a_{ps}	1.12×10^{1}
b_{ps}	7.04×10^{-1}
k_{0cg} (mol cm^{-3} min^{-1} atm^{-2} g$_{cat}^{-1}$)	1.23×10^{-1}
a_{cg}	3.04×10^{-1}
b_{cg}	8.51×10^{-1}
k_{0ht} (mol cm^{-3} min^{-1} atm^{-2} g$_{cat}^{-1}$)	3.06×10^{-1}
a_{ht}	1.41×10^{0}
b_{ht}	1.78×10^{-1}
k_{0bs} (mol cm^{-3} min^{-1} atm^{-1} g$_{cat}^{-1}$)	5.49×10^{-3}
a_{bs}	1.11×10^{1}
b_{bs}	1.59×10^{0}
$k_{0ar(6)}$ (mol cm^{-3} min^{-1} atm^{-4} g$_{cat}^{-1}$)	1.11×10^{2}
$k_{0ar(7)}$ (mol cm^{-3} min^{-1} atm^{-4} g$_{cat}^{-1}$)	7.21×10^{2}
$k_{0ar(8)}$ (mol cm^{-3} min^{-1} atm^{-4} g$_{cat}^{-1}$)	5.85×10^{2}
a_{ar}	1.41×10^{-1}
k_{0iso} (mol cm^{-3} min^{-1} atm^{-1} g$_{cat}^{-1}$)	3.00×10^{-1}
a_{iso}	1.01×10^{-1}

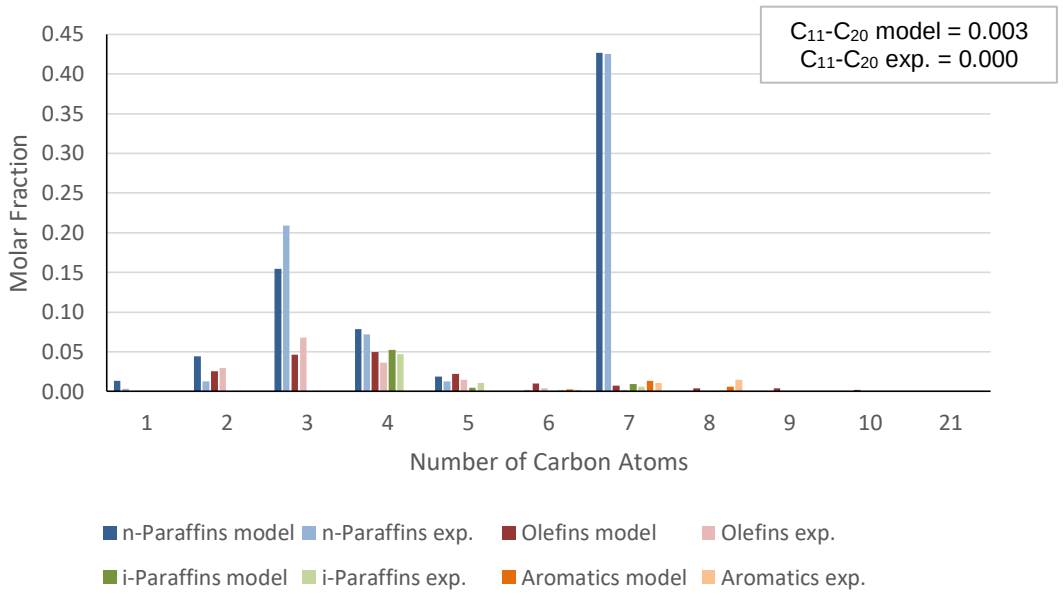

Figure 28 - Reactor outlet stream molar compositions for catalytic cracking of n-heptane comparing model and experimental results using a partial pressure of reactant in the feed of 0.42 atm.

In order to fit the model results to experimental data, the parameters value set was varied to match the se same level of conversion. Note that hydride transfer reactions involving hydrocarbons with 2 carbon atoms were not considered.

The model can produce a good qualitative prediction of the product distribution. However, the model presents significant discrepancies at C_2 and C_3. This fact is of greater importance because propane is the main product of the catalytic cracking of heptane. The main problem is the fact that the asymmetry observed in the protolytic scission between the C_3 and C_4 should be higher. However, after several simulations with different value sets for the parameters involved in the protolytic scission and hydride transfer, the asymmetry between C_3-C_4 did not suffer significant changes. The lacking of propane is offset by excess of methane and ethane mainly form secondary cracking. This fact must be related with the equation used to calculate the rate constants for the protolytic scission reaction.

The model can make an average prediction for branched paraffins and a good one for aromatics. The exception is aromatics with 8 carbon atoms because the amount and octenes predicted by the model is insufficient to produce the observed amounts and xylenes and ethyl-benzene.

Although all of these small discrepancies between the model and the experimental results, it still make a good O/P ratio prediction. The O/P ratio predicted by the model is 0.46 while the experimental is 0.41. The model's output average molecular weight was also very close to the one obtained experimentally. The model predicted an output average molecular weight of 73.81 while the one obtained experimentally was 71.85.

4.3 Model's Applicability to Other Operative Conditions and Feedstocks

In order verify the reliability of the experimental results, the molar conversion obtained experimentally was studied for 3 values of partial pressure of reactant in the feed and compared with the results obtained with the model. It is expected that the conversion decreases while the partial pressure of reactant increases. However, the experimental results can contain errors especially on the integration of the large area of the reactant peak in the chromatogram which will have a direct effect on the conversion.

4.3.1 n-Heptane

The comparison between the model conversions and experimental conversions for n-heptane are presented in Table 26.

Table 26 – Molar conversions for n-heptane obtained with the model and with experimental results.

Molar Conversion			
n-Heptane Partial Pressure in the feed (atm)	0.17	0.25	0.42
Model	59.41%	58.64%	57.32%
Experimental	59.09%	63.40%	57.47%

The conversions obtained with the model are very close to experimental conversions.

The exception is for a partial pressure of n-heptane in the feed of 0.25 atm which may indicate the occurrence of experimental errors since the value of conversion is clearly out of the conversion range.

The comparison between model and experimental results for a partial pressure of n-heptane in the feed of 0.17 and 0.25 atm are presented in Figure 29 and Figure 30, respectively.

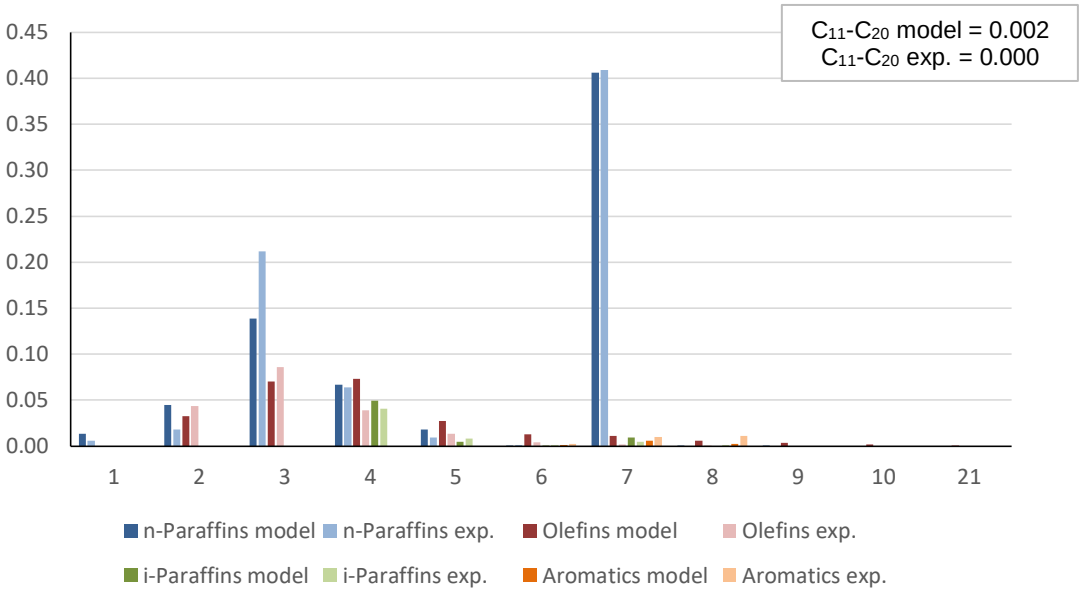

Figure 29 -Reactor outlet stream molar compositions for catalytic cracking of n-heptane comparing model and experimental results using a partial pressure of reactant in the feed of 0.17 atm.

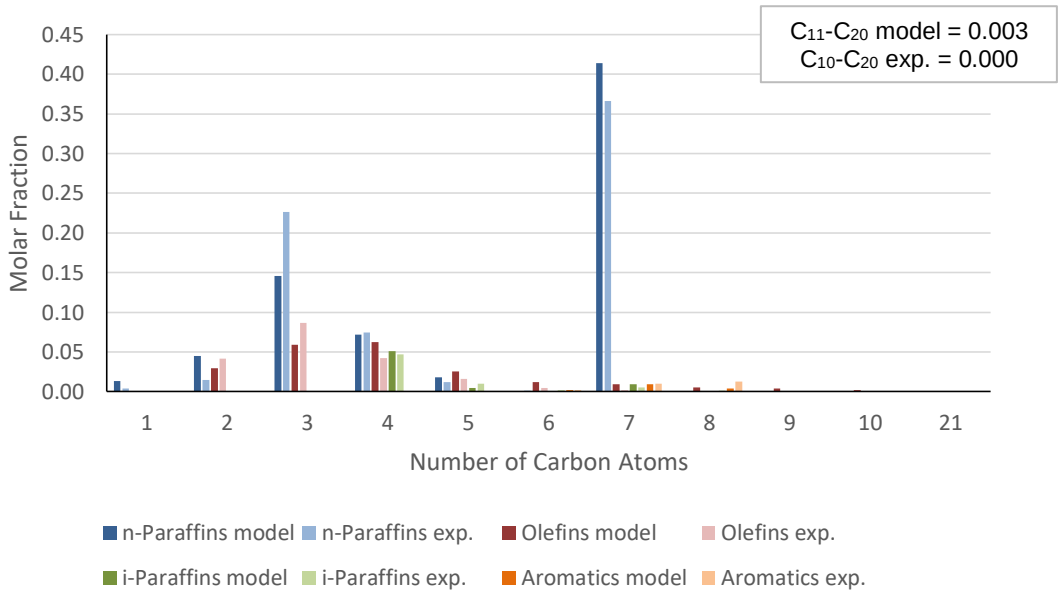

Figure 30 - Reactor outlet stream molar compositions for catalytic cracking of n-heptane comparing model and experimental results using a partial pressure of reactant in the feed of 0.25 atm.

The discrepancies obtained for partial pressures of 0.17 and 0.25 atm are very similar to the ones observed for a partial pressure of 0.42 atm as it can be observed by the output average molecular weight present in Table 27. However, the errors related to the C_2-C5 range increase when the partial pressure of reactant in the feed decreases, especially due to higher errors on propane (negative) and butenes (positive) increasing the O/P ratio which can be observed in Table 28. This can be explained by a lack of fitting on parameters related with the hydrogen transfer, chain growth or β-scission reactions.

Table 27 – Output average molecular weight for n-heptane obtained with the model and with experimental results.

Output Average Molecular Weight			
n-Heptane Partial Pressure in the Feed (atm)	0.17	0.25	0.42
Model	72.19	72.90	73.81
Experimental	69.74	68.06	71.85

Table 28 – O/P ratio for n-heptane obtained with the model and with experimental results.

O/P Ratio			
n-Heptane Partial Pressure in the Feed (atm)	0.17	0.25	0.42
Model	0.70	0.59	0.46
Experimental	0.51	0.48	0.41

4.3.2 n-Hexane

The comparison between the model conversions and experimental conversions for n-hexane are presented in Table 29.

Table 29 -– Molar conversions for n-hexane obtained with the model and with experimental results.

Molar Conversion			
n-Hexane Partial Pressure (atm) in the Feed	0.19	0.29	0.48
Model	53.94%	53.08%	51.80%
Experimental	46.85%	50.32%	44.63%

The conversions obtained with the model are close to experimental conversions but with errors that cannot be overlooked.

The conversion value for a partial pressure of n-hexane in the feed of 0.29 atm has the lowest error. However, this experimental conversion value for this partial pressure of reactant in the feed is out of the conversion range which may indicate the occurrence of experimental errors.

The comparison between model and experimental results for a partial pressure of n-hexane in the feed of 0.19, 0.29 and 0.48 are presented in Figure 31, Figure 32 and Figure 33, respectively.

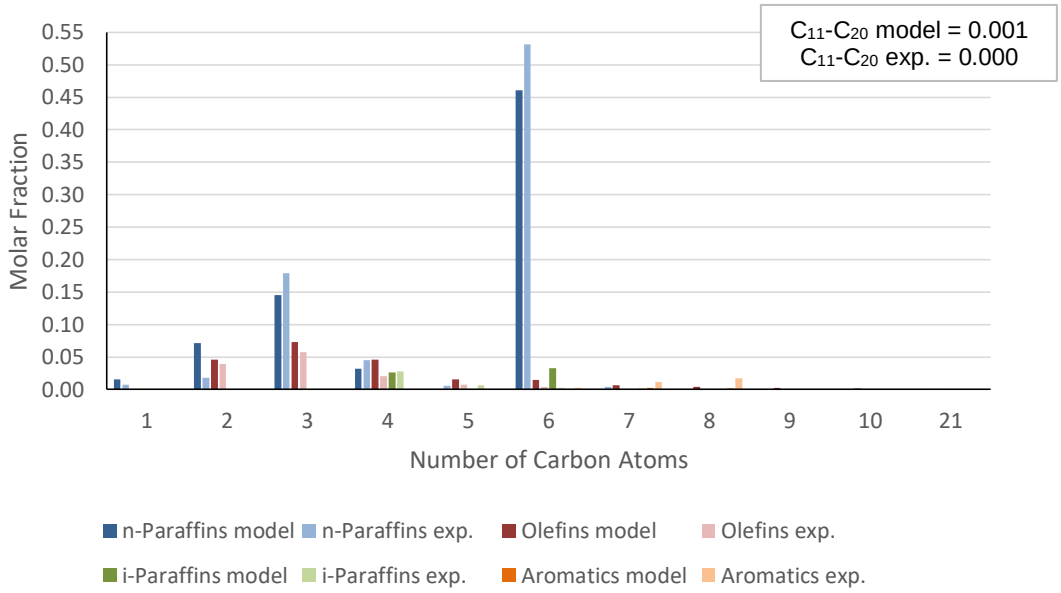

Figure 31 - Reactor outlet stream molar compositions for catalytic cracking of n-hexane comparing model and experimental results using a partial pressure of reactant in the feed of 0.19 atm.

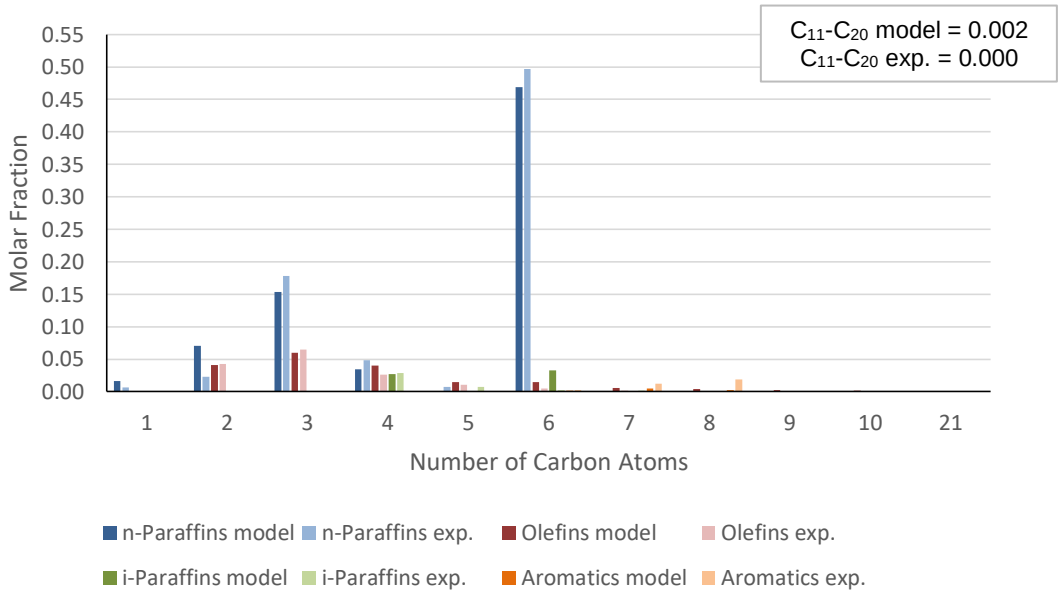

Figure 32 - Reactor outlet stream molar compositions for catalytic cracking of n-hexane comparing model and experimental results using a partial pressure of reactant in the feed of 0.29 atm.

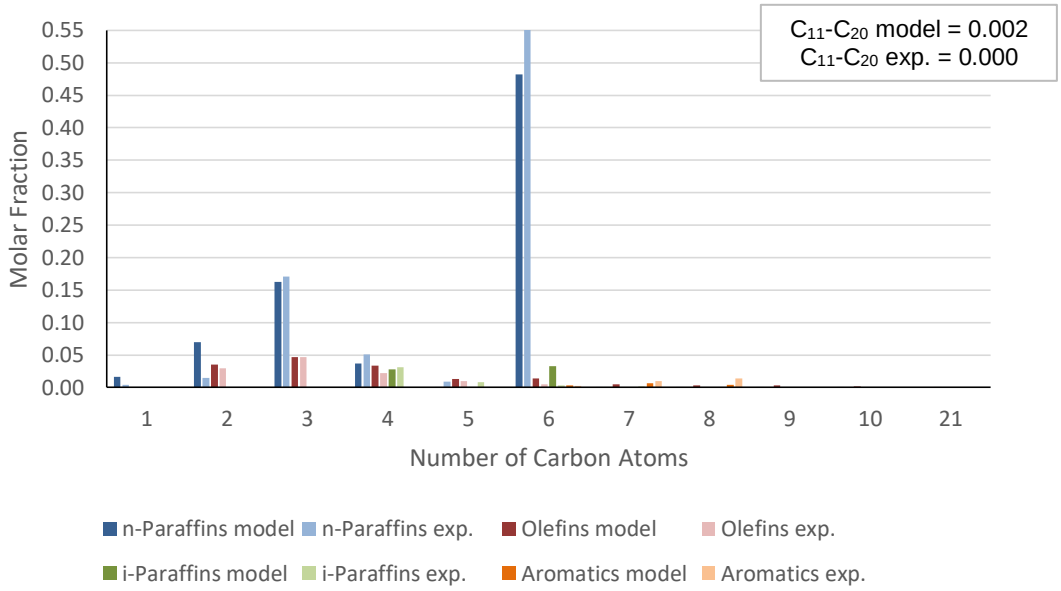

Figure 33 - Reactor outlet stream molar compositions for catalytic cracking of n-hexane comparing model and experimental results using a partial pressure of reactant in the feed of 0.48 atm.

Although the model cannot accurately predict the conversion for n-hexane, it still can make a good prediction of the product distribution as can also be observed by output average molecular weight in Table 30. However, it has a few exceptions, such as: ethane and branched hexanes.

Unlike when the reactant is n-heptane, when the reactant is n-hexane the model can make an accurate prediction for the molar fraction of propane which is the major product and this accuracy increases and the partial pressure of reactant in the feed increases. However this accuracy results of the symmetry of the primary cracking self-imposed by the model and not because it really can predict the molar fraction of propane since propane has 3 carbon atoms and hexane has 6 carbon atoms.

Both O/P ratios, predicted by the model and experimental, decreases as the partial pressure of reactant in the feed increases, as can be observed in Table 31.

Table 30 - Output average molecular weight for n-hexane obtained with the model and with experimental results.

Output Average Molecular Weight			
n-Hexane Partial Pressure in the Feed (atm)	0.19	0.29	0.48
Model	66.14	66.87	67.67
Experimental	68.79	67.45	70.01

Table 31 - O/P ratio for n-hexane obtained with the model and with experimental results.

O/P Ratio			
n-Hexane Partial Pressure in the Feed (atm)	0.19	0.29	0.48
Model	0.65	0.56	0.46
Experimental	0.44	0.50	0.39

4.3.3 n-Octane

The comparison between the model conversions and experimental conversions for n-octane are presented in Table 32.

Table 32 - Molar conversions for n-octane obtained with the model and with experimental results.

Molar Conversion			
n-Octane Partial Pressure in the Feed (atm)	0.08	0.15	0.23
Model	65.37%	64.34%	63.47%
Experimental	91.76%	83.01%	82.95%

The model completely fails to predict the conversion since the model conversions presents huge discrepancies when compared to experimental conversions. Every experimental conversion values are in the conversion range which may rule out the possibility of experimental errors.

The comparison between model and experimental results for a partial pressure of n-octane in the feed of 0.08, 0.15 and 0.23 are presented in Figure 34, Figure 35 and Figure 36, respectively.

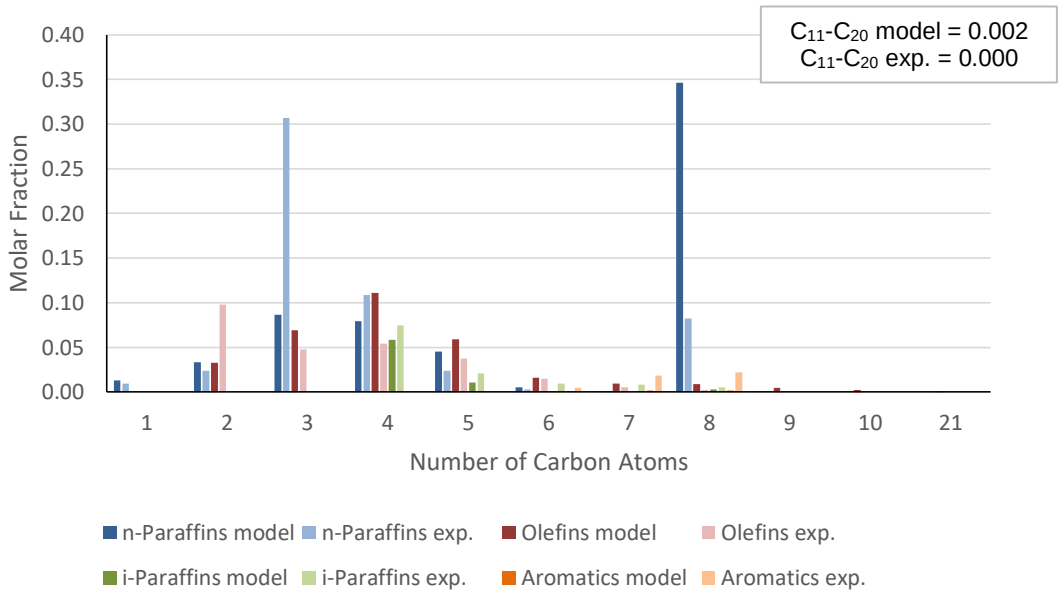

Figure 34 - Reactor outlet stream molar compositions for catalytic cracking of n-octane comparing model and experimental results using a partial pressure of reactant in the feed of 0.08 atm.

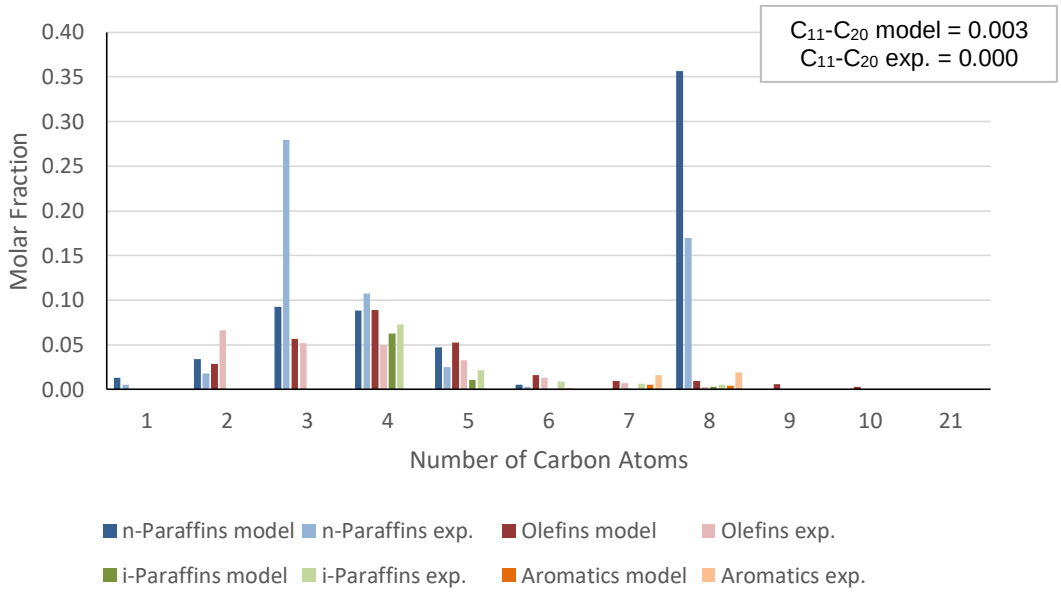

Figure 35 - Reactor outlet stream molar compositions for catalytic cracking of n-octane comparing model and experimental results using a partial pressure of reactant in the feed of 0.15 atm.

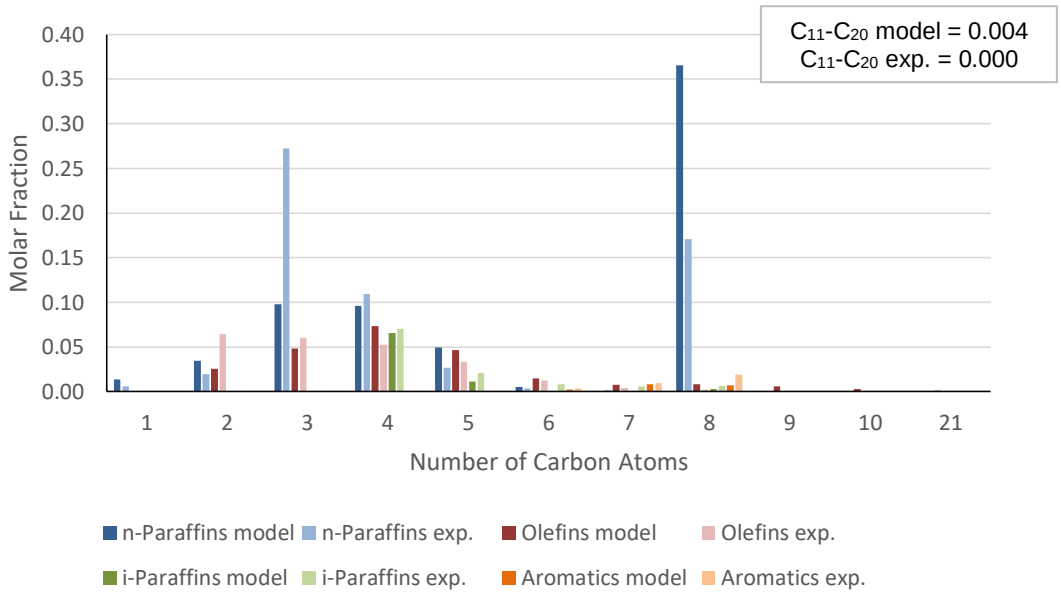

Figure 36 - Reactor outlet stream molar compositions for catalytic cracking of n-octane comparing model and experimental results using a partial pressure of reactant in the feed of 0.23 atm.

The same way model fails to predict the conversion, it fails to predict the product distribution. The major problem, as observed for n-heptane as reactant, is the fact that it cannot accurately predict the molar fraction of propane.

The output average molecular weight predicted by the model is always considerably higher than the experimental, as shown in Table 33. As the conversion is much lower in the model, the output average molecular weight will have a greater contribution of the reactant which is heavier than most of the major products.

The O/P ratio increases when the partial pressure of reactant in the feed decreases due to a general increase on olefins molar fraction and a general decrease on paraffins molar fraction. This can be related to an increase on secondary cracking which can indicate that both cracking reaction rates are too high. Also, as the reactant is not accounted in the calculation of the O/P ratio, the fact that the conversion is much lower in the model increases the model's O/P ratio value since the main differences between the model results and experimental results are the molar fractions of propane and n-octane.

Table 33 - Output average molecular weight for n-octane obtained with the model and with experimental results.

Output Average Molecular Weight			
n-Octane Partial Pressure in the Feed (atm)	0.08	0.15	0.23
Model	76.37	77.83	78.78
Experimental	56.85	63.25	62.95

Table 34 - O/P ratio for n-octane obtained with the model and with experimental results.

O/P Ratio			
n-Octane Partial Pressure in the Feed (atm)	0.08	0.15	0.23
Model	0.94	0.76	0.63
Experimental	0.44	0.40	0.41

5 Conclusions and Future Works

The study developed in this work consisted in analyzing a semi-empirical model to describe the complex kinetic network involved in catalytic cracking, The model is based on an pathways approach where the kinetic rate constants for elementary steps are obtain from empirical equations that relate the kinetic rate constant with the size and nature of the reactants and products. This work shows that these types of model present a significant potential to be used for the description of these complex networks as they can be described with some detail using a limited number of kinetic parameters. The use of a mathematical description for the kinetic parameters for a family of reactions using an empirical parameterized rationale allows us to tune the reaction so as to fit the model to existing data.

Through this work can be concluded that the protolytic scission was the reaction that had the most impact regarding the distribution of the major products, C_2-C_4.

Reactions, such as: β-scission, chain growth and hydride transfer are also important reactions, in particular regarding the O/P ratio.

The model presented in this work showed a better behavior for higher pressures of reactant. However, for feeds with reactants with more than 7 carbon atoms, the model still needs further optimization.

The parameter set of this model still needs to be better fitted to the existent data. All the fitting was done by manual search. An automatic fitting would perhaps a better choice.

The equation used to calculate the protolytic scission rate constants need some adjustments. These adjustments could involve the addition of another parameter or the modification of the equation in order to enable the model to make better predictions of the molar fraction of propane, which is the major product for the catalytic cracking of small paraffins. The deviations in this lump increase considerably with the number of carbon atoms of a pure reactant in the feed, as the model was not able to capture the asymmetry of the product distribution in relation to the point corresponding to half the size of the original hydrocarbon

Before the implementation of this model to real gas oil feedstocks, more lumps and more reactions must be introduced first for a better understanding of this complex reaction network which is the catalytic cracking.

The experimental results used to develop this model has H-ZSM5 as catalyst. This zeolite has a low tendency to promote coke formation which was observed in this work. However, the fact that the model can be tuned to calculate the formation of coke, the addition of a parameter which accounts for the deactivation by coke would be of great use when applying this model to real gas oil feedstocks.

THIS PAGE WAS INTENTIONALLY LEFT BLANK

6 References

[1] F. Ribeiro, “Refininig processes: evolution and futur of oil refinery,” 2015.

[2] F. Ribeiro, “OIL INDUSTRY Evolution and perspectives,” 2015.

[3] S. Oruji, R. Khoshbin, and R. Karimzadeh, “Preparation of hierarchical structure of Y zeolite with ultrasonic-assisted alkaline treatment method used in catalytic cracking of middle distillate cut: The effect of irradiation time,” Fuel Process. Technol., vol. 176, no. January, pp. 283–295, 2018.

[4] B. W. Wojciechowski and A. Corma, Catalytic cracking: *Catalysts, Chemistry, and Kinetics*, Chemical Industries. Marcel Dekker, Inc., 1986.

[5] BP Energy Economics, “2018 BP Energy Outlook 2018 BP Energy Outlook”, 2018.

[6] J. Shankleman, “The Electric Car Revolution Is Accelerating.” [Online]. Available: https://www.bloomberg.com/news/articles/2017-07-06/the-electric-car-revolution-is-accelerating.

[7] Alan Tovey, “Diesel cars face ‘collapse’ to just 15pc of the market.” [Online]. Available: https://www.telegraph.co.uk/business/2018/01/09/diesel-cars-face-collapse-just-15pc-market/.

[8] A. Kumar and M. T. Klein, “Molecule-based modeling of gasoil fluid catalytic cracking”, ACS Div. Fuel Chem. Prepr., vol. 44, no. 3, pp. 485–489, 1999.

[9] X. Chen, T. Li, L. Xin, Y. Yang, H. Shan, and C. Yang, “Inductive effect of basic nitrogen compounds on coke formation during the catalytic cracking process”, Catal. Commun., vol. 74, pp. 95–98, 2016.

[10] R. Radeghbeigi, Fluid Catalytic Cracking Handbook, 3rd ed. Butterworth Heinemann, 2012.

[11] W. Letzsch, “Fluid catalytic cracking (FCC)”, *Handbook of Petroleum Processing*, 2006, pp. 239–286.

[12] E. T. C. Vogt and B. M. Weckhuysen, “Fluid catalytic cracking: recent developments on the grand old lady of zeolite catalysis”, Chem. Soc. Rev., vol. 44, no. 20, pp. 7342–7370, 2015.

[13] N. Rahimi and R. Karimzadeh, “Catalytic cracking of hydrocarbons over modified ZSM-5 zeolites to produce light olefins: A review”, Appl. Catal. A Gen., vol. 398, no. 1–2, pp. 1–17, 2011.

[14] A. I. Hussain, A. M. Aitani, M. Kubů, Jнc. Čejka, and S. Al-Khattaf, “Catalytic cracking of Arabian Light VGO over novel zeolites as FCC catalyst additives for maximizing propylene yield”, Fuel, vol. 167, pp. 226–239, 2016.

[15] M. A. Den Hollander, M. Wissink, M. Makkee, and J. A. Moulijn, “Gasoline conversion: Reactivity towards cracking with equilibrated FCC and ZSM-5 catalysts”, Appl. Catal. A Gen., vol. 223, no. 1–2, pp. 85–102, 2002.

[16] Z. Chen, J. Xu, Y. Fan, G. Shi, and X. Bao, “Reaction mechanism and kinetic modeling of hydroisomerization and hydroaromatization of fluid catalytic cracking naphtha”, Fuel

Process. Technol., vol. 130, no. C, pp. 117–126, 2015.

[17] F. R. Ribeiro, F. Alvarez, C. Henriques, F. Lemos, J. M. Lopes, and M. F. Ribeiro, “Structure-activity relationship in zeolites”, J. Mol. Catal. A. Chem., vol. 96, no. 3, pp. 245–270, 1995.

[18] P. O. Fritz and J. H. Lunsford, “The effect of sodium poisoning on dealuminated Y-type zeolites”, J. Catal., vol. 118, no. 1, pp. 85–98, 1989.

[19] M. Gackowski et al., “Hierarchical zeolites Y obtained by desilication: Porosity, acidity and catalytic properties”, Microporous Mesoporous Mater., vol. 263, pp. 282–288, 2018.

[20] a Corma, V. Fornes, J. B. Monton, and a V Orchilles, “Catalytic Cracking of Alkanes on Large Pore, High Sio2/Al2o3 Zeolites in the Presence of Basic Nitrogen-Compounds - Influence of Catalyst Structure and Composition in the Activity and Selectivity”, Ind. Eng. Chem. Res., vol. 26, no. 5, pp. 882–886, 1987.

[21] B. Liu, K. Xie, S. C. Oh, D. Sun, Y. Fang, and H. Xi, “Direct synthesis of hierarchical USY zeolite for retardation of catalyst deactivation”, Chem. Eng. Sci., vol. 153, pp. 374–381, 2016.

[22] B. A. Williams, S. M. Babitz, J. T. Miller, R. Q. Snurr, and H. H. Kung, “The roles of acid strength and pore diffusion in the enhanced cracking activity of steamed Y zeolites”, Appl. Catal. A Gen., vol. 177, no. 2, pp. 161–175, 1999.

[23] T. Long-Xiang, Z. Feng-Mei, L. Dong-Fan, and Z. Lu-Bin, “Characteristics of the poisoning effect of nickel deposited on USY zeolite”, Appl. Catal. A, Gen., vol. 91, no. 2, pp. 67–80, 1992.

[24] U. J. Etim, B. Xu, R. Ullah, and Z. Yan, “Effect of vanadium contamination on the framework and micropore structure of ultra stable Y-zeolite”, J. Colloid Interface Sci., vol. 463, pp. 188–198, 2016.

[25] U. J. Etim, B. Xu, P. Bai, R. Ullah, F. Subhan, and Z. Yan, “Role of nickel on vanadium poisoned FCC catalyst: A study of physiochemical properties”, J. Energy Chem., vol. 25, no. 4, pp. 667–676, 2016.

[26] F. C. Whitmore, “Mechanism of the Polymerization of Olefins by Acid Catalysts”, Ind. Eng. Chem., vol. 26, no. 1, pp. 94–95, 1934.

[27] A. Kogelbauer and J. A. Lercher, “Cracking of light alkanes over HNaK erionites”, J. Catal., vol. 125, no. 1, pp. 197–206, 1990.

[28] J. Abbot, “Role of Brønsted and Lewis acid sites during cracking reactions of alkanes”, Appl. Catal., vol. 47, no. 1, pp. 33–44, 1989.

[29] W. F. Pansing, “The Catalytic Cracking of Hexadecane—Effects of Impurities, Olefins, and Steam,” J. Phys. Chem., vol. 69, no. 2, pp. 392–399, 1965.

[30] B. S. Greensfelder, H. H. Voge, and G. M. Good, “Catalytic and Thermal Cracking of Pure Hydrocarbons: Mechanisms of Reaction”, Ind. Eng. Chem., vol. 41, no. 11, pp. 2573–2584, 1949.

[31] W. O. Haag and R. M. Dessau, “Duality of Mechanism for Acid-Catalyzed Paraffin Cracking”, Proceedings of the 8th International Congress on Catalysis, 1984, vol. 2, p.

305.

[32] S. Kotrel, H. Knözinger, and B. C. Gates, “The Haag-Dessau mechanism of protolytic cracking of alkanes”, Microporous Mesoporous Mater., vol. 35–36, pp. 11–20, 2000.

[33] A. Corma and A. V. Orchillés, “Current views on the mechanism of catalytic cracking”, Microporous Mesoporous Mater., vol. 35–36, pp. 21–30, 2000.

[34] J. Sommer, D. Habermacher, and M. Hachoumy, “The H/D exchange reaction occurring at low temperature between small alkanes and D20 exchanged solid acids. III. The role of alkenes and carbenium ions as reaction intermediates”, vol. 146, pp. 193–205, 1996.

[35] J. Sommer, R. Jost, and M. Hachoumy, “Activation of small alkanes on strong solid acids: Mechanistic approaches”, Catal. Today, vol. 38, no. 3, pp. 309–319, 1997.

[36] J. Sommer, A. Sassi, M. Hachoumy, R. Jost, A. Karlsson, and P. Ahlberg, “Similarities and differences in activation of small alkanes by liquid and solid strong acids: An NMR, MS, and UV spectroscopic study”, J. Catal., vol. 171, no. 2, pp. 391–397, 1997.

[37] Y. V. Kissin, “Chemical mechanism of hydrocarbon cracking over solid acidic catalysts”, J. Catal., vol. 163, no. 1, pp. 50–62, 1996.

[38] Y. V. Kissin, “Primary products in hydrocarbon cracking over solid acidic catalysts under very mild conditions: Relation to cracking mechanism”, J. Catal., vol. 180, no. 1, pp. 101–105, 1998.

[39] S. T. Sie, “Acid-Catalyzed Cracking of Paraffinic Hydrocarbons. 1. Discussion of Existing Mechanisms and Proposal of a New Mechanism”, Ind. Eng. Chem. Res., vol. 31, no. 8, pp. 1881–1889, 1992.

[40] S. T. Sie, “Acid-Catalyzed Cracking of Paraffinic Hydrocarbons. 2. Evidence for the Protonated Cyclopropane Mechanism from Catalytic Cracking Experiments”, Ind. Eng. Chem. Res., vol. 32, no. 3, pp. 397–402, 1993.

[41] L. Riekerti and J. Q. Zhou, “Kinetics of cracking of n-decane and n-hexane on zeoiites H-ZSM-5 and HY in the temperature range 500 to 780 K”, J. Catal., vol. 137, no. 2, pp. 437–452, 1992.

[42] D. B. Lukyanov, V. I. Shtral, and S. N. Khadzhiev, “A kinetic model for the hexane cracking reaction over H-ZSM-5”, J. Catal., vol. 146, no. 1, pp. 87–92, 1994.

[43] G. Giannetto, S. Sansare, and M. Guisnet, “Influence of acid site densities on the mode of alkane cracking”, J. Chem. Soc., Chem. Commun., no. 16, pp. 1302–1303, 1986.

[44] B. A. Watson, M. T. Klein, and R. H. Harding, “Mechanistic modeling of n-heptane cracking on HZSM-5”, Ind. Eng. Chem. Res., vol. 35, no. 5, pp. 1506–1516, 1996.

[45] I. Pitault, D. Nevicato, M. Forissier, and J. R. Bernard, “Kinetic model based on a molecular description for catalytic cracking of vacuum gas oil”, Chem. Eng. Sci., vol. 49, no. 24, pp. 4249–4262, 1994.

[46] V. W. Weekman, “A model of catalytic cracking conversion in fixed, moving, and fluid-bed reactors”, Ind. Eng. Chem. Process Des. Dev., vol. 7, no. 1, pp. 90–95, 1968.

[47] V. W. Weekman and D. M. Nace, “Kinetics of catalytic cracking selectivity in fixed, moving, and fluid bed reactors”, AIChE J., vol. 16, no. 3, pp. 397–404, 1970.

[48] L. L. Oliveira and E. Biscaia, “Catalytic cracking kinetic models. Parameter estimation and model evaluation”, Ind. Eng. Chem. Res., vol. 28, no. 3, pp. 264–271, 1989.

[49] L.-S. Lee, Y.-W. Chen, T.-N. Huang, and W.-Y. Pan, “Four-lump kinetic model for fluid catalytic cracking process”, Can. J. Chem. Eng., vol. 67, no. 4, pp. 615–619, 1989.

[50] A. Gupta and D. Subba Rao, “Model for the performance of a fluid catalytic cracking (FCC) riser reactor: Effect of feed atomization”, Chem. Eng. Sci., vol. 56, no. 15, pp. 4489–4503, 2001.

[51] J. Ancheyta-Juárez, F. López-Isunza, and E. Aguilar-Rodríguez, “5-Lump Kinetic Model for Gas Oil Catalytic Cracking”, Appl. Catal. A Gen., vol. 177, no. 2, pp. 227–235, 1999.

[52] J. Corella and E. Frances, “Analysis of the Riser Reactor of a Fluid Catalytic Cracking Unit”, Fluid Catal. Crack. II concepts Catal. Des. Vol. 452 ACS Symp. Ser., vol. 452, no. 6, p. 165, 1991.

[53] G. M. Bollas, A. A. Lappas, D. K. Iatridis, and I. A. Vasalos, “Five-lump kinetic model with selective catalyst deactivation for the prediction of the product selectivity in the fluid catalytic cracking process”, Catal. Today, vol. 127, no. 1–4, pp. 31–43, 2007.

[54] M. M. Sugungun, I. M. Kolesnikov, V. M. Vinogradov, and S. I. Kolesnikov, “Kinetic modeling of FCC process”, Catal. Today, vol. 43, no. 3–4, pp. 315–325, 1998.

[55] C. Chen, B. Yang, J. Yuan, Z. Wang, and L. Wang, “Establishment and solution of eight-lump kinetic model for FCC gasoline secondary reaction using particle swarm optimization”, Fuel, vol. 86, no. 15, pp. 2325–2332, 2007.

[56] Q. Yang et al., “CFD investigation of hydrodynamics, heat transfer and cracking reactions in a large-scale fluidized catalytic cracking riser”, Appl. Math. Model., vol. 40, no. 21–22, pp. 9378–9397, 2016.

[57] R. R. Pinto, “Kinetic Modelling of Catalytic Cracking Reactions”, Instituto Superior Técnico, 2004.

[58] P. Borges, “Acidity-Activity Correlations for the Transformation of Hydrocarbons Over ZSM-5 Zeolites”, Instituto Superior Técnico, 2005.

A. Appendix I – Values drawn from Spartan'06 to calculate the isomerization equilibrium constants.

Table A. 1 - Enthalpies of formation, entropies of formation, free energy of Gibbs of formation and isomerization equilibrium constants for butanes.

Compound	ΔH (J/mol)	ΔS (J/mol.K))	ΔG (j/mol)	K
n-butane	3.66×10^5	3.00×10^2	2.77×10^5	-
2-methylpropane	3.65×10^5	2.95×10^2	2.77×10^5	1.04

Table A. 2 - Enthalpies of formation, entropies of formation, free energy of Gibbs of formation and isomerization equilibrium constants for pentanes.

Compound	ΔH (J/mol)	ΔS (J/mol.K))	ΔG (j/mol)	K
n-Pentane	4.45×10^5	3.33×10^2	3.45×10^5	-
2-methylbutane	4.44×10^5	3.33×10^2	3.45×10^5	1.25
2,2-dimethylpropane	4.42×10^5	3.26×10^2	3.44×10^5	1.65

Table A. 3 - Enthalpies of formation, entropies of formation, free energy of Gibbs of formation and isomerization equilibrium constants for hexanes.

Compound	ΔH (J/mol)	ΔS (J/mol.K))	ΔG (j/mol)	K
n-hexane	5.23×10^5	3.67×10^2	4.14×10^5	-
2-methylpentane	5.23×10^5	3.62×10^2	4.15×10^5	0.61
3-methylpentane	5.22×10^5	3.67×10^2	4.13×10^5	1.40
2,2-dimethylButane	5.21×10^5	3.54×10^2	4.16×10^5	0.55
2,3-dimethylbutane	5.21×10^5	3.67×10^2	4.12×10^5	2.53

Table A. 4 - Enthalpies of formation, entropies of formation, free energy of Gibbs of formation and isomerization equilibrium constants for heptanes.

Compound	ΔH (J/mol)	ΔS (J/mol.K))	ΔG (j/mol)	K
n-heptane	5.99×10^5	3.79×10^2	4.86×10^5	-
2-methylhexane	6.02×10^5	3.95×10^2	4.84×10^5	2.32
3-methylhexane	6.02×10^5	3.95×10^2	4.84×10^5	2.32
2,2-dimethylpentane	5.99×10^5	3.89×10^2	4.83×10^5	3.08
2,3-dimethylpentane	6.01×10^5	3.98×10^2	4.82×10^5	5.20
2,4-dimethylpentane	6.01×10^5	3.82×10^2	4.87×10^5	0.83
3,3-dimethylpentane	6.00×10^5	3.80×10^2	4.87×10^5	0.82
3-ethylpentane	6.02×10^5	3.92×10^2	4.85×10^5	1.65
2,2,3-trimethylbutane	5.96×10^5	3.66×10^2	4.87×10^5	0.84

Table A. 5 - Enthalpies of formation, entropies of formation, free energy of Gibbs of formation and isomerization equilibrium constants for octanes.

Compound	ΔH (J/mol)	ΔS (J/mol.K))	ΔG (j/mol)	K
n-octane	6.78×10^5	4.11×10^2	5.55×10^5	-
2-methyheptane	6.80×10^5	4.27×10^2	5.53×10^5	2.72
3-methylheptane	6.80×10^5	4.30×10^2	5.52×10^5	3.75
4-methylheptane	6.80×10^5	4.32×10^2	5.51×10^5	5.36
2,2-dimethylhexane	6.75×10^5	4.04×10^2	5.54×10^5	1.43
2,3-dimethylhexane	6.80×10^5	4.25×10^2	5.53×10^5	2.49
2,4-dimethylHexane	6.80×10^5	4.20×10^2	5.54×10^5	1.55
2,5-dimethylhexane	6.80×10^5	4.19×10^2	5.55×10^5	1.28
3,3-dimethylhexane	6.76×10^5	4.00×10^2	5.57×10^5	0.45
3,4-dimethylhexane	6.77×10^5	4.05×10^2	5.57×10^5	0.62
3-ethylhexane	6.81×10^5	4.24×10^2	5.54×10^5	1.53
2,2,3-trimethylpentane	6.78×10^5	4.09×10^2	5.56×10^5	0.76
2,2,4-trimethylpentane	6.75×10^5	3.90×10^2	5.59×10^5	0.24
2,3,3-trimethylpentane	6.78×10^5	4.35×10^2	5.49×10^5	15.51
2,3,4-trimethylpentane	6.79×10^5	4.11×10^2	5.57×10^5	0.57
3-ethyl,2-methylpentane	6.75×10^5	3.88×10^2	5.59×10^5	0.20
3-ethyl,3-methylpentane	6.79×10^5	4.07×10^2	5.58×10^5	0.35

B. Appendix II – Parameter values used in the study of the equations used to obtain rate constants.

Table B. 1 - Previous reactions parameter values used in chain growth.

Parameter	Value
k_{0ps} (mol cm^{-3} min^{-1} atm^{-1} g$_{cat}^{-1}$)	1.31×10^{-2}
a_{ps}	1.12×10^{1}
b_{ps}	7.04×10^{-1}

Table B. 2 - Previous reactions parameter values used in hydride transfer study.

Parameter	Value
k_{0ps} (mol cm^{-3} min^{-1} atm^{-1} g$_{cat}^{-1}$)	1.31×10^{-2}
a_{ps}	1.12×10^{1}
b_{ps}	7.04×10^{-1}
k_{0cg} (mol cm^{-3} min^{-1} atm^{-2} g$_{cat}^{-1}$)	1.23×10^{-1}
a_{cg}	3.04×10^{-1}
b_{cg}	8.51×10^{-1}

Table B. 3 - Previous reactions parameter values used in β-scission study.

Parameter	Value
k_{0ps} (mol cm^{-3} min^{-1} atm^{-1} g$_{cat}^{-1}$)	1.31×10^{-2}
a_{ps}	1.12×10^{1}
b_{ps}	7.04×10^{-1}
k_{0cg} (mol cm^{-3} min^{-1} atm^{-2} g$_{cat}^{-1}$)	1.23×10^{-1}
a_{cg}	3.04×10^{-1}
b_{cg}	8.51×10^{-1}
k_{0ht} (mol cm^{-3} min^{-1} atm^{-2} g$_{cat}^{-1}$)	1.53×10^{0}
a_{ht}	1.41×10^{0}
b_{ht}	1.78×10^{-1}

Table B. 4 - Previous reactions parameter values used in aromatic formation study.

Parameter	Value
k_{0ps} (mol cm^{-3} min^{-1} atm^{-1} g$_{cat}^{-1}$)	1.31×10^{-2}
a_{ps}	1.12×10^{1}
b_{ps}	7.04×10^{-1}
k_{0cg} (mol cm^{-3} min^{-1} atm^{-2} g$_{cat}^{-1}$)	1.23×10^{-1}
a_{cg}	3.04×10^{-1}
b_{cg}	8.51×10^{-1}
k_{0ht} (mol cm^{-3} min^{-1} atm^{-2} g$_{cat}^{-1}$)	1.53×10^{-1}
a_{ht}	1.41×10^{0}
b_{ht}	1.78×10^{-1}
k_{0bs} (mol cm^{-3} min^{-1} atm^{-1} g$_{cat}^{-1}$)	5.49×10^{-3}
a_{bs}	1.11×10^{1}
b_{bs}	1.59×10^{0}

Table B. 5 - Previous reactions parameter values used in isomerization study.

Parameter	Value
k_{0ps} (mol cm^{-3} min^{-1} atm^{-1} g$_{cat}^{-1}$)	1.31×10^{-2}
a_{ps}	1.12×10^{1}
b_{ps}	7.04×10^{-1}
k_{0cg} (mol cm^{-3} min^{-1} atm^{-2} g$_{cat}^{-1}$)	1.23×10^{-1}
a_{cg}	3.04×10^{-1}
b_{cg}	8.51×10^{-1}
k_{0ht} (mol cm^{-3} min^{-1} atm^{-2} g$_{cat}^{-1}$)	1.53×10^{-1}
a_{ht}	1.41×10^{0}
b_{ht}	1.78×10^{-1}
k_{0bs} (mol cm^{-3} min^{-1} atm^{-1} g$_{cat}^{-1}$)	5.49×10^{-3}
a_{bs}	1.11×10^{1}
b_{bs}	1.59×10^{0}
$k_{0ar(6)}$ (mol cm^{-3} min^{-1} atm^{-4} g$_{cat}^{-1}$)	2.78×10^{2}
$k_{0ar(7)}$ (mol cm^{-3} min^{-1} atm^{-4} g$_{cat}^{-1}$)	8.01×10^{2}
$k_{0ar(8)}$ (mol cm^{-3} min^{-1} atm^{-4} g$_{cat}^{-1}$)	5.85×10^{2}
a_{ar}	1.41×10^{-1}